FPN 3

EG&G INC.

TECHNICAL REPORT

NUMBER B-3256
EGG-1183-280
15 MARCH 1966

PROGRESS REPORT IMPULSIVE LOADING BY MAGNETIC FIELDS PHASE 2

Prepared by

R. Brundage
J. Farber

Prepared for

The Sandia Corporation

SYSTEMS DIVISION

EDGERTON, GERMESHAUSEN & GRIER, INC.

EG&G INC.

EG&G INC.

TABLES

ILLUSTRATIONS

FIGURE

EG&G INC.

FIGURE

CHAPTER 1
INTRODUCTION

The activities by the Advanced Research Department of Edgerton, Germeshausen & Grier, Inc. for the Livermore Laboratory of Sandia Corporation reported in EG&G Technical Report B-3147, 28 September 1965, have been extended and elaborated. Ways and means of achieving the technical objectives described in the Sandia Corporation letter of 7 October 1965 have been investigated, and the following report presents the results of these investigations.[1]

Chapter 2 describes the experimental methods, Chapter 3 describes the techniques devised for impulsive magnetic field loading of cylindrical and flat structures, Chapter 4 presents selected analyses of the experimental results, and Chapter 5 contains plans for continued effort.

The analyses contained in report B-3147 are included herein only by reference.

The EG&G pulse-power bank has been used throughout this set of experiments as a source of stored electrical energy. A selection of load coils was available for generation of high-transient magnetic fields. Early experiments were performed with a single-turn beryllium-copper coil 2.863 inches long and having an inside diameter of 3.015 inches. Later experiments took advantage of the greater magnetic efficiency of a closely coupled multiple-turn coil.[2] The beryllium-copper concentrator used with the latter coil has the same inside dimensions as the single-turn coil. A few experiments were performed with a larger single-turn coil to accommodate the 7-inch diameter phenolic samples forwarded by Sandia Corporation. This coil, of cast aluminum, has a 10-inch length and a 10-inch inside diameter.

2.1 VOLTAGE AND CURRENT MEASUREMENTS

Measurements of voltage induced across the load coil were made by two methods. Initially, 1000 to 1 attenuation probes were located at each end of the load coil, and the attenuated signal was displayed through a differential amplifier on a Tektronix Type 555 dual-beam oscilloscope located in a shielded room. It was found that this arrangement resulted in spurious signal pickup. Acquisition of an additional Tektronix Type 507 high-voltage oscilloscope permitted relocating the high-sensitivity portion of the circuitry several feet from the load coil. At high bank voltages, attenuation by a factor of 10 was still required, but spurious signal pickup was satisfactorily avoided.

Measurements of the rate of change of current in the load coil and hence of the rate of change of the magnetic field within the coil were made by measurement of the voltage induced in a small single-turn pickup loop oriented on the central plane of the load coil in the volume permeated by

the magnetic field. A loop area as small as 0.005 square centimeter was found to give adequate signal voltage. Loop areas as large as 0.070 square centimeter were used when space permitted. The pickup loop signal voltage was typically displayed on the Tektronix Type 555 dual-beam oscilloscope. One loop of zero area was fabricated to check the signal pickup of the twisted leads used to carry the signal to a coaxial cable outside the coil. The unwanted signal pickup was found to be satisfactorily negligible.

2.2 HIGH-SPEED PHOTOGRAPHY

For high-speed photography of the behavior of the workpieces under impulse of a magnetic field transient, use was made of a Kerr Framing Camera manufactured by Electro-Optical Systems. This camera and associated electronics provides 6 exposures of the same object with time delays between exposures variable from 0 to 50 microseconds. Available exposure times were 0.2 and 1.0 microseconds. The output triggers were adjustable in time by observation on a Tektronix Type 545 oscilloscope and were recorded photographically to provide the necessary time correlation between photographs and voltage data. The maximum image diameter at the film plane of the Kerr Framing Camera is approximately one inch. Accordingly, with 3-inch diameter objects, an optical system was chosen that provided a 3 to 1 minification. A typical optical arrangement is illustrated in Figure 1. It was sufficiently flexible that the object focal plane could be adjusted from the central plane of the coil to the front edge for cases where front-lighting was more desirable than back-lighting. Illumination was provided by a Type 1532-B Strobolume Xenon flash lamp, with additional capacitance and inductance to provide about 50 joules stretched over a period of at least 100 microseconds. Because the time of onset of the light flash is uncertain by 20 to 30

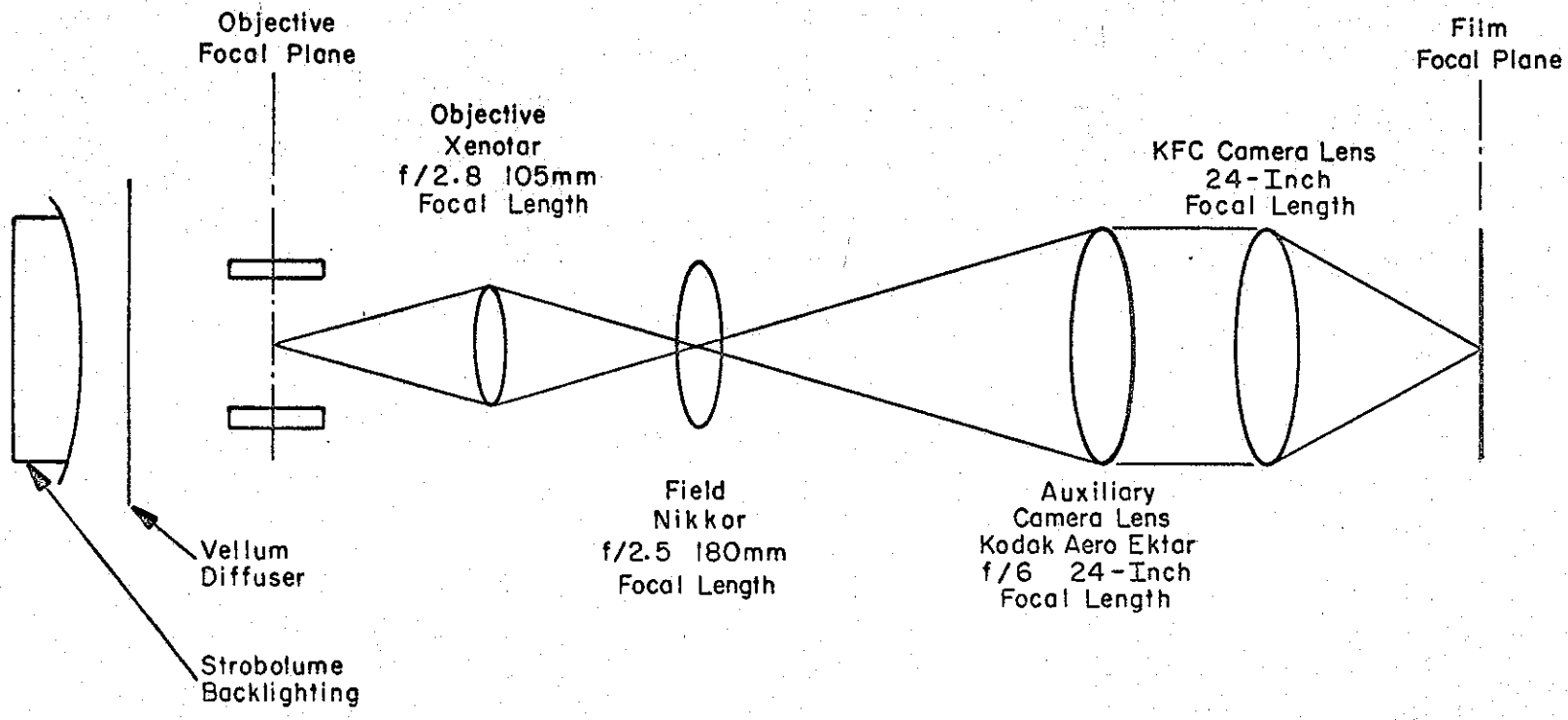

Figure 1. Typical optical system for interior photography of moving workpieces.

EG&G INC.

microseconds, all experiments were performed with the light flash as a fiducial marker. The light flash was detected photoelectrically by an EG&G FIDU sensor. The latter provided four-trigger outputs to trigger the pulse-power bank, the camera control unit, and the oscilloscopes. Figure 2 is a block diagram showing a typical trigger-circuit arrangement. The modified light source and optical system provided adequate illumination at the film plane for satisfactory photography. With the 0.2-microsecond exposure, use of the diffuser was not possible even with the fastest film available, Royal-X Panchromatic or Polaroid Type 57. With the 1-microsecond exposure, use of the vellum diffuser was practicable. In addition, it was sometimes desirable to use the slower Polaroid Type 52 for some of the frames. With some of the experimental geometries, it is not possible to avoid extraneous light from arcing. The extent of this is unpredictable, and satisfactory photographic records are sometimes not obtained with Polaroid. In these cases it is more desirable, although less convenient, to use negative sheet film; e.g., Royal-X Panchromatic.

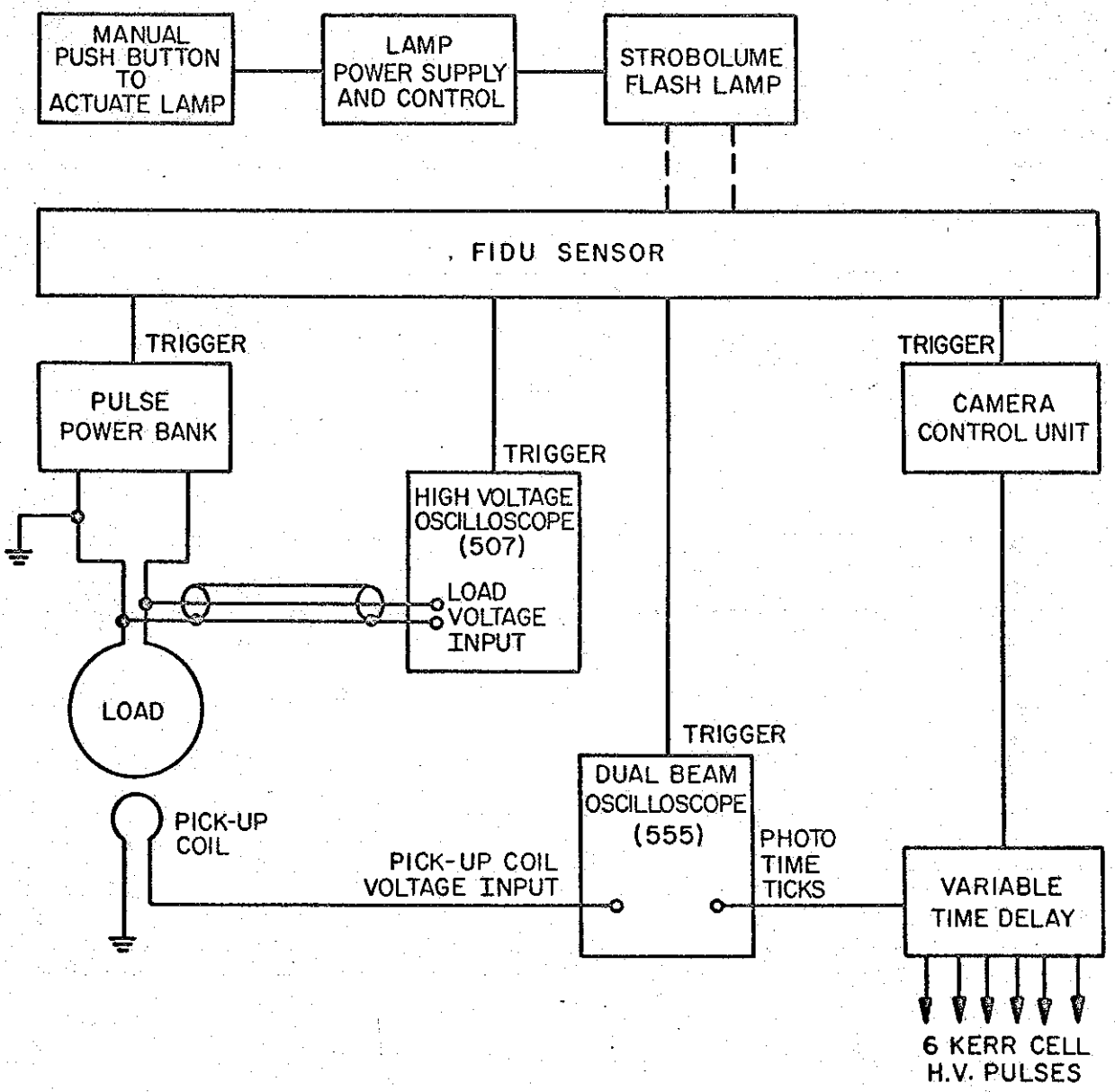

Figure 2. Typical arrangement of electronics for control and recording.

CHAPTER 3
IMPULSIVE LOADING OF CYLINDRICAL AND FLAT STRUCTURES WITH MAGNETIC FIELDS

Initial experiments were conducted with the magnetic field loading uniform over entire cylindrical surfaces. Later experiments were directed towards loading 120 degrees of cylindrical surfaces first in a uniformly radial manner and second, according to a cosine law with the maximum loading at the center of the 120-degree sector. A few involved loading of small flat surfaces. Selected results of each type of experiment are presented below.

3.1 UNIFORM LOADING OVER ENTIRE CYLINDER

For this purpose, the single-turn beryllium-copper coil was employed across the load plates. Both aluminum and copper cylinders were swaged. Copper cylinders, 0.008-inch thick, were formed by butt-soldering a copper sheet into a cylindrical shape. Aluminum cylinders were cut to length from a 3-inch outside diameter tube with a 0.028-inch wall thickness. The most satisfactory photographic results were achieved with cylinders cut to the same length as the coil. Typical results obtained are illustrated in Figure 3. The workpiece was aluminum. The bank was fired at 19.4 kilovolts or approximately 31 kilojoules of stored energy. The photographs shown were taken at the following times after the initial voltage excursion: 5, 9.5, and 13.5 microseconds. Between the first and third photograph, the approximate average radius decreased by 3.3 millimeters, indicating an average radial velocity of about 3.9×10^4 cm/sec. Of interest is the shock wave just visible in the second and third photographs. The average velocity of the shock wave over that 4-microsecond interval was approximately 1.1×10^5 cm/sec. This implies a peak velocity for the aluminum wall on the same order of magnitude. Precise instantaneous velocity measurements by these techniques are not possible. However, photographs taken at +7 and +8.5 microseconds together with that at +9.5 microseconds (Figure 3b) indicate that the

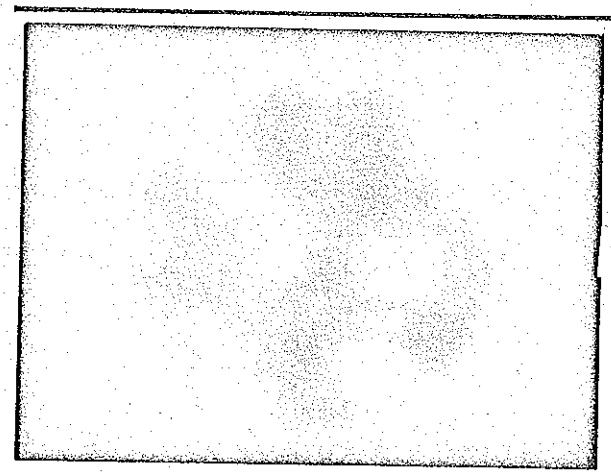

(a) Bank to +5 microseconds

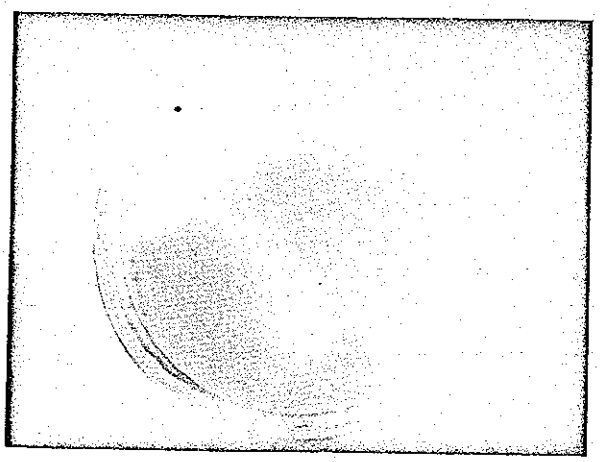

(b) Bank to +9.5 microseconds

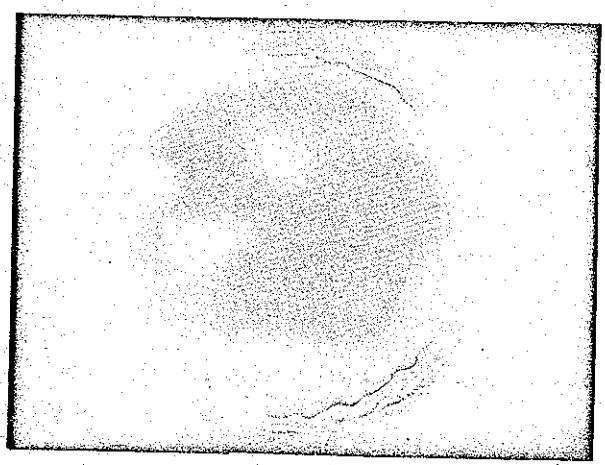

(c) Bank to +12.5 microseconds

Figure 3. Three sequential views of the aluminum workpiece, shown at approximately full scale, in the process of swaging. Shock wave is visible in (b) and (c).

average velocity of the wall was approximately 6×10^4 cm/sec. The average velocity during the period from +9.5 to +13.5 microseconds was down to 3×10^4 cm/sec.

Of interest is that at +9.5 microseconds a high order of buckling has occurred with a spacing between neighbor buckles of approximately 0.43 centimeter. The question arises as to what would be the simultaneity of impact if a target structure had been located at the radius reached at +9.5 microseconds; that is, at the approximate time of maximum velocity. At +9.5 microseconds the radius of the buckled cylinder is approximately 0.92 of the initial inside radius. Hence, the material contained in an arc distance of 0.43 centimeter at +9.5 microseconds must have been contained initially in an arc distance greater in the ratio of 1 to 0.92, or 0.47 centimeter. If one approximates the cross section of each buckle by a triangle, then the base of the triangle is 0.43 centimeter, and the sum of the other two sides is 0.47 centimeter. The height of the triangle, therefore, is 0.095 centimeter. At the observed radial velocity of 6×10^4 cm/sec, all points on the interior surface of the buckled cylinder would arrive at the radius reached at +9.5 microseconds within a time interval of approximately 1.5 microseconds.

3.2 UNIFORM RADIAL LOADING OVER 120 DEGREES

To investigate the behavior of collapsing structures under conditions of uniform radial loading over a limited sector of a cylinder, two different methods were applied. The first was selected for 3-inch diameter metal cylinders supplied by EG&G; the second was devised to accommodate the 7-inch diameter phenolic cylinders supplied by Sandia.

3.2.1 Three-inch Diameter Metal Cylinders. For these structures, recourse was taken to the device of selecting a relatively

thick-wall aluminum tube and reducing the outside radius over a 120-degree sector by milling parallel to the axis of the cylinder until the thin wall was approximately one skin-depth thick at a typical bank frequency under load. A typical experimental geometry is shown in Figure 4. For these experiments, the single-turn load coil was replaced by the multiple-turn coil whose concentrator dimensions duplicated those of the single-turn coil. Typical results of the use of this technique are shown in Figure 5. The exposures were made at 11, 25, and 35 microseconds after the onset of the voltage excursion. In this example, the pulse power bank was charged up only to 10 kilovolts, corresponding to 8.25 kilojoules. Buckling is discernible in Figure 5a and becomes more serious and somewhat irregular at later times in Figures 5b and 5c. The irregularities in the buckling may have been due to possible residual irregularities in the milling process. The average radial velocity of the thin-walled section has been calculated to be 1.5×10^4 cm/sec from 0 to +11 microseconds, 1.6×10^4 cm/sec from +11 to +25 microseconds, and 1.2×10^4 cm/sec from +25 to +35 microseconds. The thin section commenced shearing prior to +11 microseconds, developing an arc observable in Figure 5b. The electrical circuit was probably effectively open by +50 microseconds, although some arcing was still observed as late as +64 microseconds.

The following experiment was identical in geometry to the preceding one except that a strip of 0.002-inch thick mylar approximately one inch wide was placed in the central region of the thin-wall sector. Sequential views of the motion of the thin-wall sector and the mylar are shown in Figure 6. The times of making the exposures are identical with those applying to Figure 5. Apparently the natural stiffness of the mylar resulted in it initially being in contact with the aluminum near the long edges of the mylar. The mylar takes on the buckling of the aluminum as it develops and as the aluminum comes into contact with the mylar. The conditions

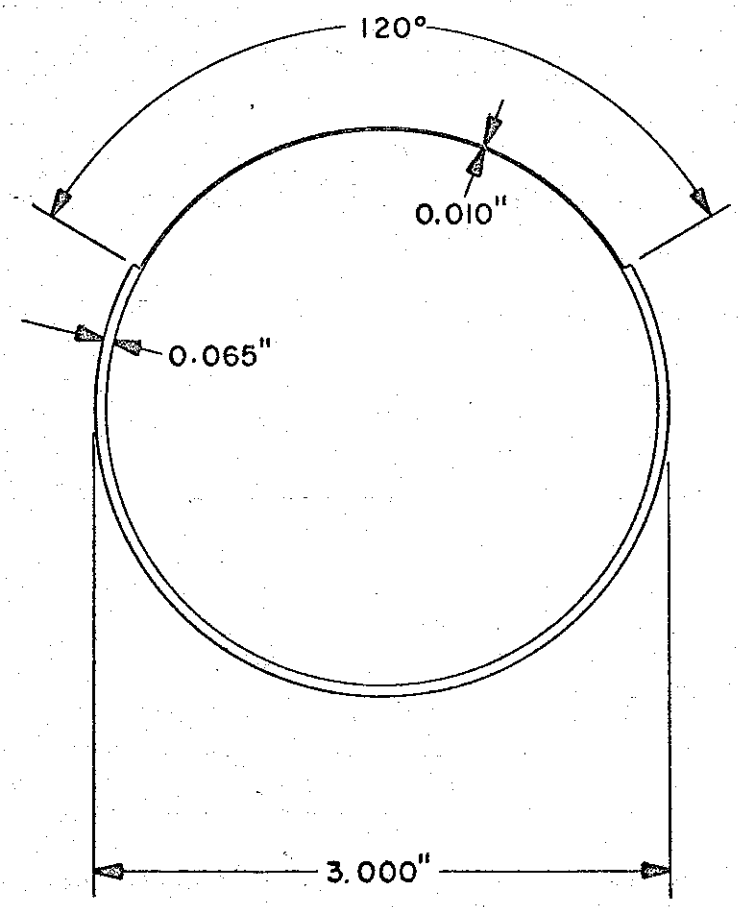

Figure 4. Typical geometry for uniform radial loading by magnetic fields; stock material is an aluminum tube.

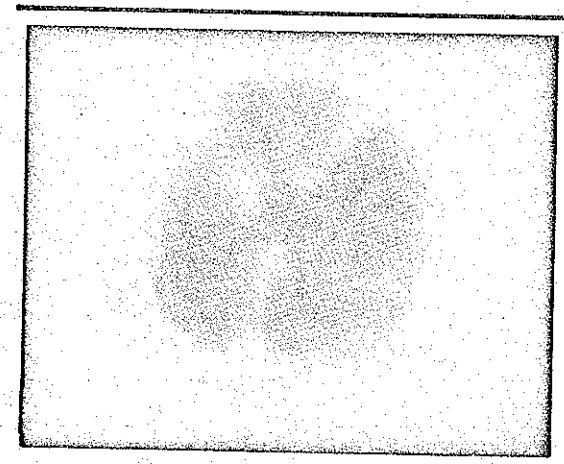

(a) Bank to +11 microseconds

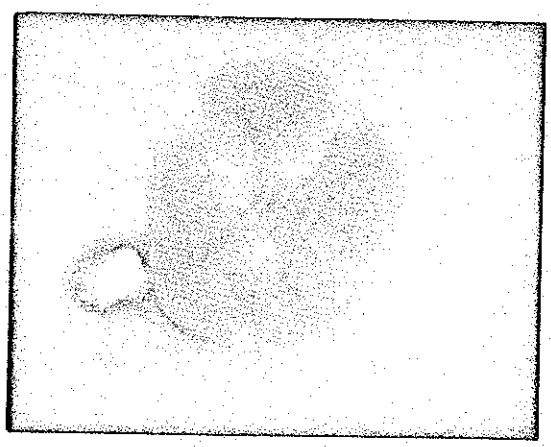

(b) Bank to +25 microseconds

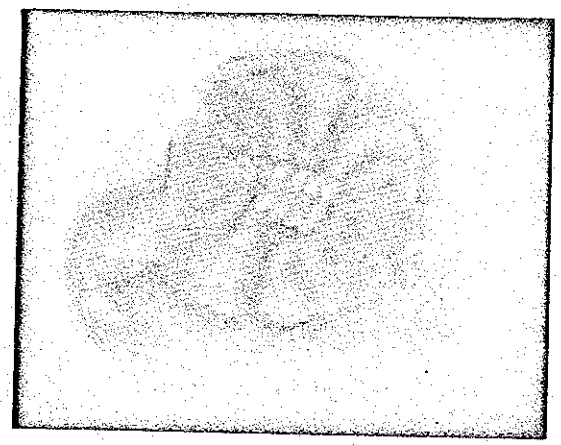

(c) Bank to +35 microseconds

Figure 5. Three sequential views of an aluminum tube, thin walled over a 120-degree sector, in the process of radial motion.

(a) Bank to +11 microseconds

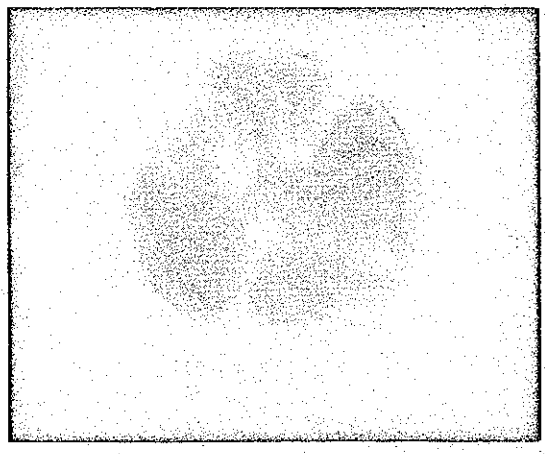

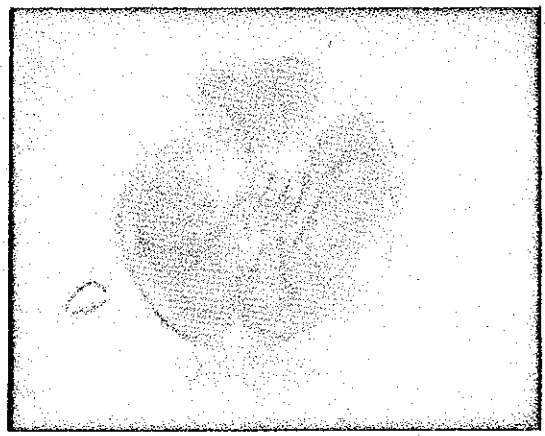

(b) Bank to +25 microseconds

(c) Bank to +35 microseconds

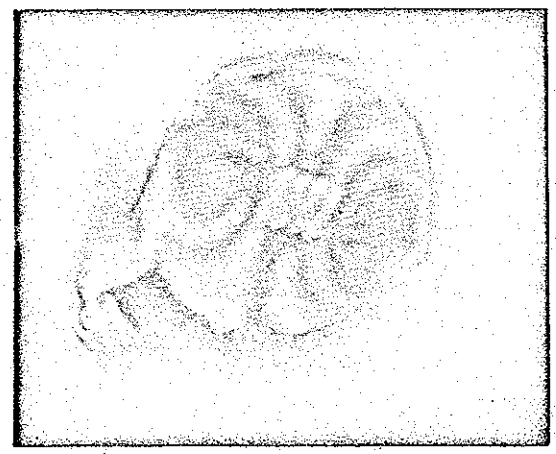

Figure 6. Three sequential views of an aluminum tube, thin walled over a 120-degree sector, in motion. Thin sheet of mylar is superposed on the thin aluminum sector.

of discharge of the bank were the same, 10 kilovolts, as the preceding event. The observed average velocities are comparable in the two cases.

3.2.2 Seven-inch Diameter Phenolic Cylinders. The experience described in Sections 3.1 and 3.2.1 indicates that good simultaneity can be achieved in impulsive radial loading over a part of a cylindrical surface provided that the initial separation of the impacting materials is small compared to the cylinder radius and provided that the initial thickness of the flyer plate is uniform. Accordingly, efforts were undertaken to load impulsively the phenolic cylinders supplied by Sandia Corporation. As received, these cylinders were 7 inches OD, 0.5-inch wall thickness and 9 inches long. Five cylinders were supplied, one of which showed a defect in lamination. The other four appeared in good initial condition.

To provide full loading over 120 degrees of the cylinder samples and zero loading over the remaining 240 degrees, the geometry illustrated in Figure 7 was chosen. The load coil illustrated was available from other work. Its dimensions, 10 inches square in longitudinal inside cross-section, were convenient for the purpose of providing room for the 240-degree retaining ring shown. The thickness chosen for the retaining ring was adequate to avoid radial motion in that sector at the full bank energy. The flux concentrators shown were inserted to minimize the added inductances. With the flux concentrators in place, the inductance of this geometry was approximately 20 nanohenries, slightly less than half the internal bank inductance of 43 nanohenries.

Preliminary diagnostic measurements made in this geometry utilized a 9-inch length for the aluminum sheet. Polaroid photographic observations throughout the first 100 microseconds showed some buckling of the sheet, but barely perceptible motion. Because the impulse given by the magnetic pressure is inversely proportional to the square of the

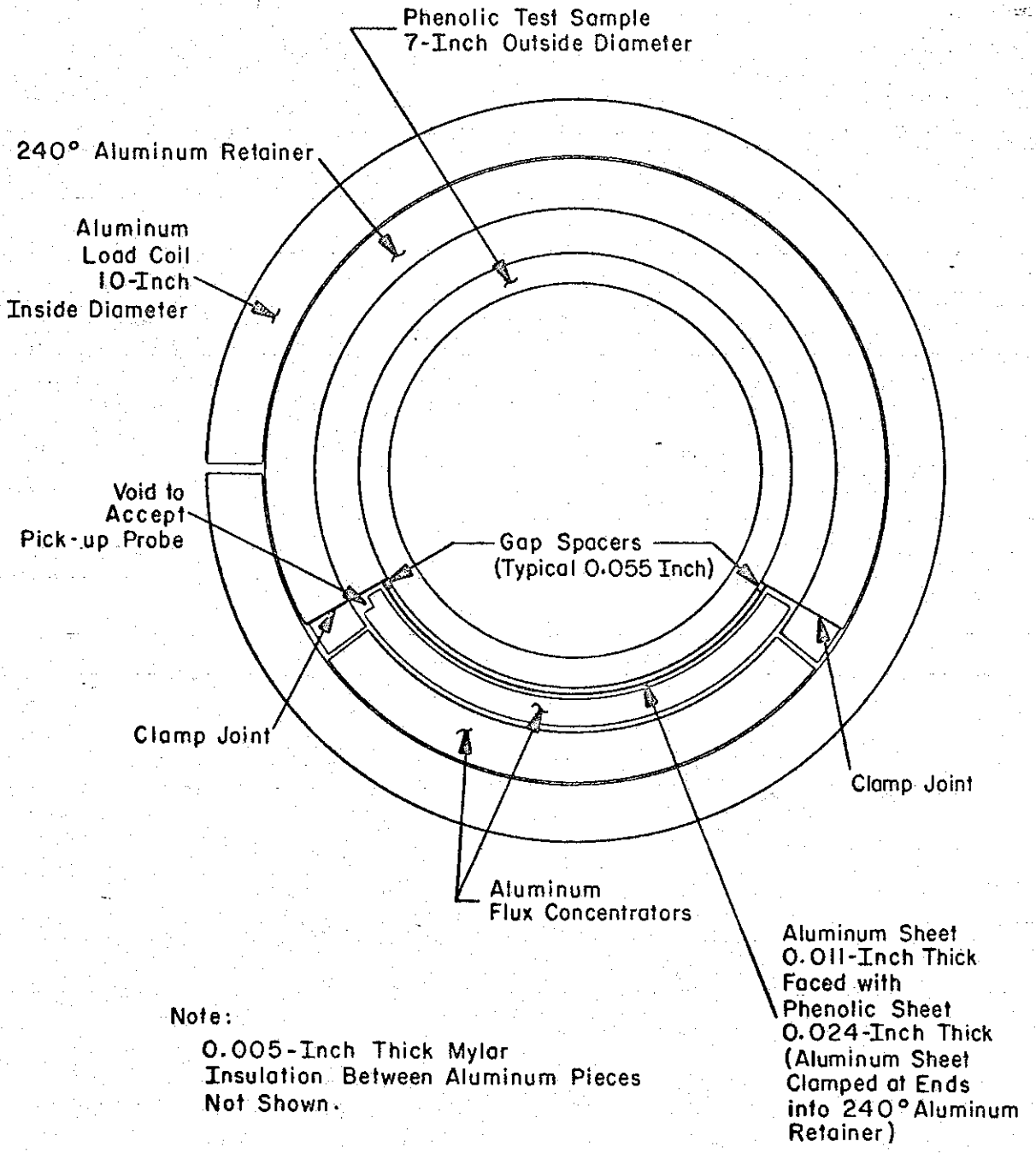

Figure 7. Low-inductance geometry for 120-degree impulsive loading phenolic sheet on the phenolic cylinder.

length, a significant decrease in the length of the aluminum sheet was indicated.[3] A length of 2 inches was selected, resulting in an impulse increase by a factor of slightly over 20. At this length satisfactory results were achieved. Observed average velocities of the aluminum sheet (without phenolic facing) were about 0.5 mm/μsec over the first twelve microseconds of the impulse. On the basis of these results, the 2-inch length was retained for the aluminum sheet and applied in the geometry of Figure 7.

The initial test of phenolic loading on a phenolic test sample was made with one of the 9-inch long samples supplied. The 2-inch length of aluminum with phenolic facing was oriented centrally with respect to the length of the cylinder. The bank was discharged at 19.5 kilovolts, corresponding to a bank energy of 31.4 kilojoules. The resultant spallation, which is confined to the interior surface of the cylinder, is shown in Figure 8.

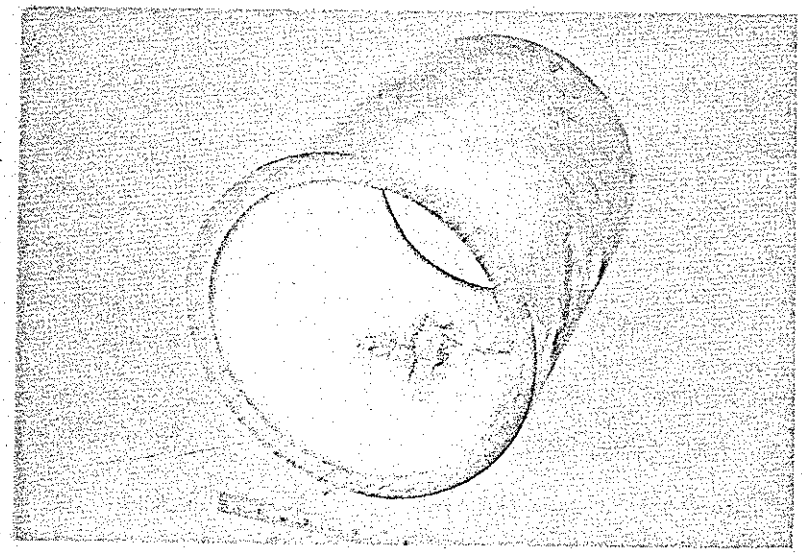

Figure 8. Interior spallation of the phenolic cylinder impulsively loaded over a 2-inch length and 120 degrees of exterior surface.

Polaroid photography over the first 112 microseconds indicates that the spallation commenced between 12 and 32 microseconds after the initial excursion of the bank. Inspection of the damage indicated that it had been minimized by the constraints of the adjacent unloaded material.

The remaining phenolic cylinders were, therefore, cut into 2-inch lengths so that the full length of the test sample would be impulsively loaded. Two examples of these tests are illustrated in Figure 9. The region of interest is the bottom third of the central one of the three cylinders evident in the photographs. To assist the reader in interpreting the photographs, it should be noted that the center of the central cylinder is slightly higher than those of the front and back cylinders. With back-lighting, its lower surface casts a shadow on the front cylinder. The luminous material, shown in the later photographs, is hot aluminum from the ends of the aluminum driver sheet. This material escaped through the gaps between the cylinders.

Two views are shown in Figure 9 of each of test samples, one taken at +31 microseconds, the other at +111 microseconds. One of the test samples was impulsively loaded with the bank discharged at close to full energy, the other at half the energy of the first. In both cases spallation is evident at +31 microseconds. In neither case was spallation evident in photographs taken at +11 microseconds (not shown).

The complete effects of impulsive loading at full bank energy are illustrated in before-and-after views in Figure 10. The residual unspalled but delaminated material is clearly evident. The spalled residue is not included.

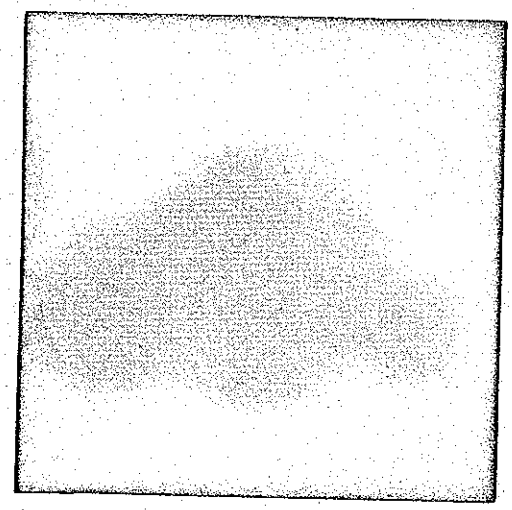

(a) 31 kilojoules at +31 microseconds

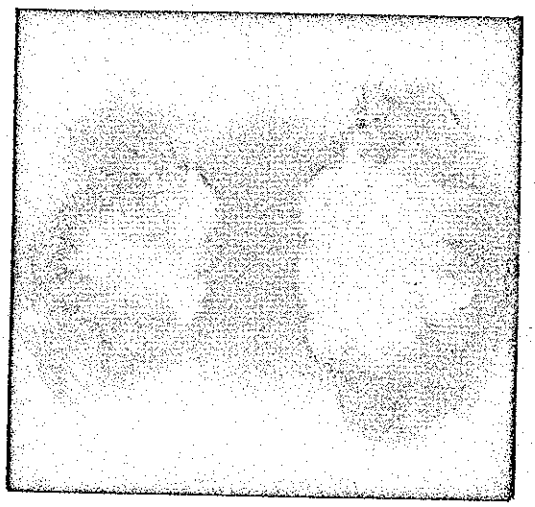

(c) 15.5 kilojoules at +31 microseconds

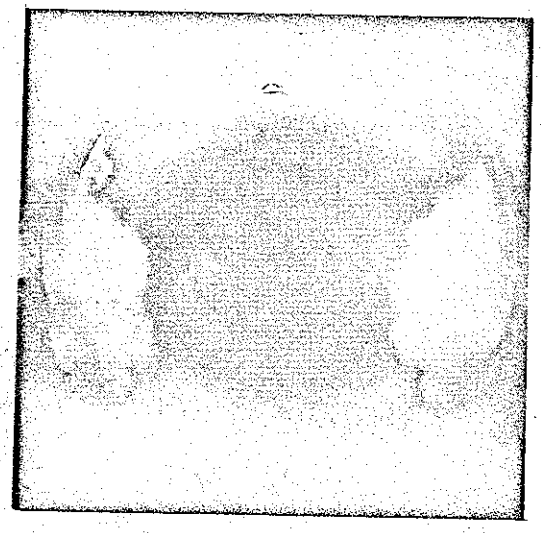

(b) 31 kilojoules at +111 microseconds

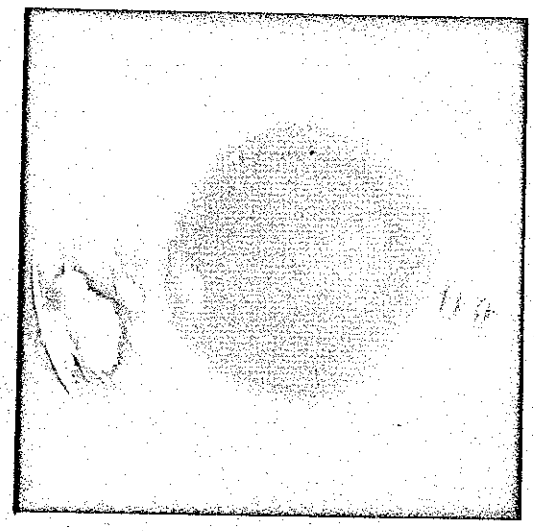

(d) 15.5 kilojoules at +111 microseconds

Figure 9. Sequential views of spallation damage in phenolic cylinders.

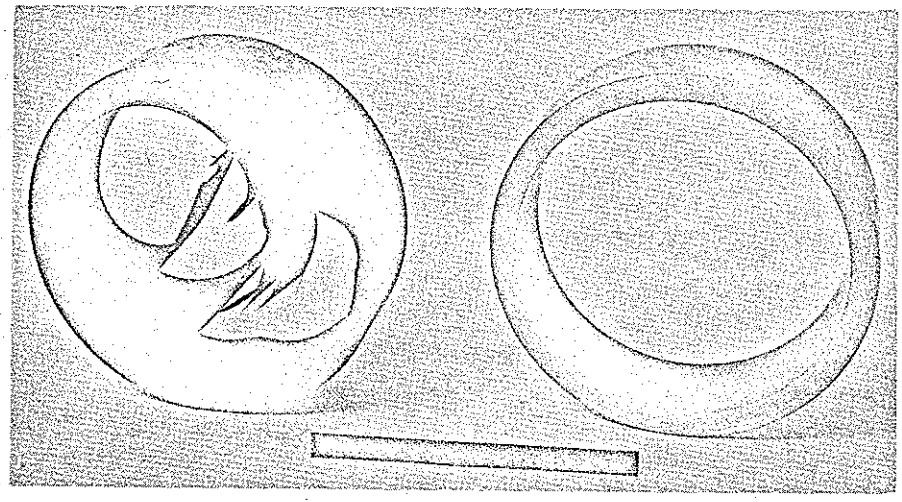

Figure 10. Before and after views of spallation and delamination damage of the phenolic cylinder impulsively loaded at almost full bank energy.

3.3 COSINE LAW LOADING OVER A 120-DEGREE SECTOR

Efforts have been directed towards use of transient magnetic field pressures to achieve loading over semi-cylindrical surfaces that approximates a plane wave. As a practical matter, efforts have been limited, at least initially, to providing the desired loading over a 120-degree sector with the maximum at the center. For simultaneity of loading of 1 microsecond by the use of workpieces traveling at 1×10^5 cm/sec, the surface of the workpiece that strikes the cylindrical target must have the same radius as the target with a tolerance of approximately a millimeter. To provide the desired cosine distribution of loading, no element of the moving cylindrical surface can have a velocity vector different in direction or amplitude from any other element. The pressure of the transient magnetic field is exerted normal to the surface of the workpiece. To meet the velocity vector criterion requires that the surface of the workpiece driven by the magnetic field be flat. With these constraints in mind, experimental

discharges have been made with a variety of materials to determine the requirements for meeting the criteria satisfactorily. A typical experimental geometry is illustrated in Figure 11.

The so-called "drive workpiece" shown in Figure 11 is designed to translate the linear motion of the flat surface driven by the copper sheet into linear motion of the cylindrical surface towards contact with the target cylinder. At the same time, to approximate desired velocities of impact (approximately 10^5 cm/sec) its mass must be comparable with or significantly less than that of the driving copper sheet. Attempts have been made with two light-weight materials, a foamed plastic with a density of approximately 0.1 gram per cubic centimeter and a fiberglas honeycomb with a density of approximately 0.065 gram per cubic centimeter. Neither of these materials possess the necessary rigidity to transmit the required impulse to the cylindrical surfaces. Data recently supplied by the manufacturer of honeycomb materials indicates that the compressive strength is inadequate by a factor of at least 10 to transmit the required pressures. In both cases, deformation of the cylindrical surface has taken place prior to significant acceleration.

Further efforts in this direction have been suspended until more profitable avenues of approach appear.

3.4 IMPULSIVE LOADING OF FLAT STRUCTURES WITH MAGNETIC FIELDS

An experimental geometry very similar to that described in Section 3.3 was considered to be potentially useful for impulsive loading of flat structures. If one replaces the annular cylindrical retaining segment shown in Figure 11 with a solid cylindrical segment with the flat parallel to the flat of the copper driver, then it is, in principle, possible

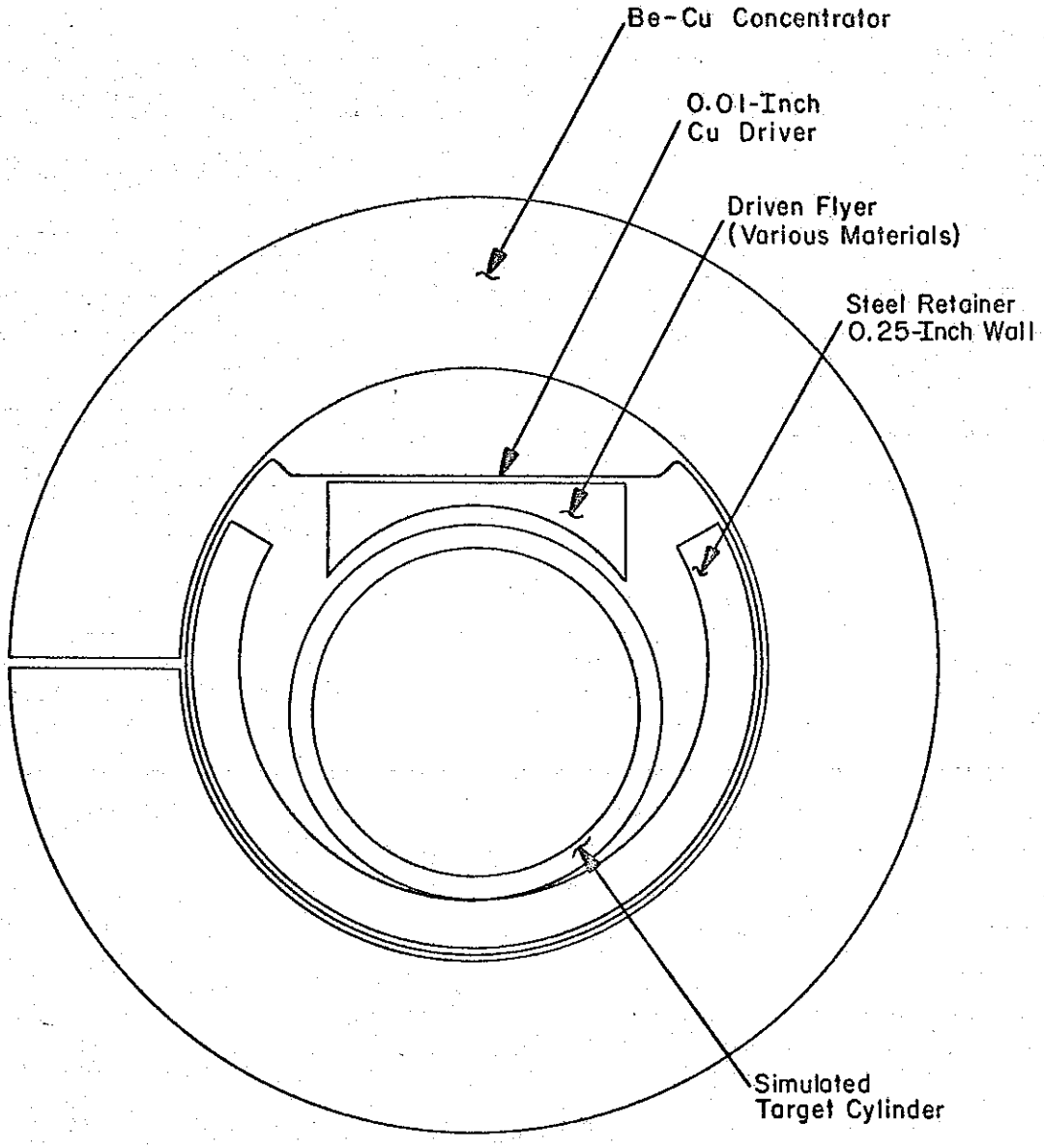

Note:
Mylar Insulation Between Metal Surfaces
Not Shown.

Figure 11. Typical experimental geometry for cosine law loading of cylindrical surfaces.

to load impulsively small flat targets supported off the surface of the retainer. The loading would be provided by flat-flyer plates driven by the copper. Several such attempts were made with both metal and phenolic targets. The results were ambiguous in that no satisfactory means was found to protect the target plate from damage after loading in the process of crushing the material; e. g., styrafoam which was placed between the target plate and the retainer. Further efforts in this direction should be oriented towards an open geometry in which the target sample would be free to slow down in flight through air over a distance of some inches or feet before its motion was otherwise arrested. A suitable open geometry will be described in Chapter 5, Plans for Continued Effort.

CHAPTER 4
ANALYSIS AND INTERPRETATION OF SOME EXPERIMENTAL RESULTS

Detailed analysis and interpretation have been made on one example of each of three different classes of experiments described in Chapter 3, based on the theory of time-varying LRC circuits.[4] The first of these analyses pertains to the case of a flat copper flyer plate accelerated towards the flat of a solid cylindrical segment (Section 3.4). The second pertains to one attempt to simulate cosine law loading (Section 3.3). The third analysis relates to radial impulsive loading of a limited sector (approximately 120 degrees) of a phenolic cylinder (Section 3.2.2).

4.1 FLAT COPPER FLYER PLATE

All the impulsive loading tests, involving flat copper flyer plates, were conducted using a multiple-turn coil and flux concentrator.[2] The configuration of this assembly introduces considerable additional inductance into the circuit. This serves to decrease both the ringing frequency and the current in the primary or main circuit. However, the multiple-turn windings also act as a transformer, and the current in the single-turn flux concentrator is increased by a factor equal to the turns ratio. Originally, it was thought that this gain in current would more than offset the disadvantages incurred by slowing down the bank, but calculations based on empirical evidence have since shown this reasoning to be fallacious.

As discussed in the previous progress report, useful information can be obtained from studying accurate oscilloscope traces of the current through, and the voltage across, the workpiece.[5] The term workpiece is herewith defined to describe the ensemble that consists of the inner side of the flux concentrator, the flyer plate, and any other metal surfaces that are inserted between the test cylinder and the flux concentrator for the purpose of reducing inductance. These oscilloscope traces are

particularly valuable as diagnostic tools when the inductance of the workpiece predominates over the sum of all other inductances in the circuit. Then, any changes in the workpiece inductance that are effected by the action of the magnetic pressure pulse driving the flyer plate, serve to modify appreciably the current flowing in the circuit. These changes can then be monitored by the scopes and compared with the non time-varying inductance case. Unfortunately, the EG&G 33-kilojoule bank has an internal inductance of 45 nanohenries, far greater than that of the typical workpiece. The use of the multiple-turn flux concentrator introduces additional inductance in excess of 100 nanohenries into the circuit and further reduces the efficacy of the scope traces. In spite of this, useful information has been obtained using these diagnostic techniques.

4.1.1 Calibration Tests. Initially, the problem of accurately measuring the current had to be solved. The current is indirectly measured by a small pickup loop that is placed in the spacing between the flux concentrator and the flyer plate. This loop measures the induced voltage, which is produced by a time-varying magnetic field, according to Faraday's Law. From Ampere's Law this magnetic field is directly proportional to the current in the circuit, and one can theoretically correlate the measured loop voltage, V_p, to the actual current, I.

In practice, one can relate V_p to the time rate of change of current, dI/dt, only if the inductance of the pickup loop is accurately known. An accurate determination of the loop inductance from its geometry is most difficult to obtain, especially when the loop area is small. The inductance, a measure of the magnetic flux that passes through the loop, is critically dependent on the orientation of the loop with respect to the direction of the magnetic field lines, in addition to the loop area. For solenoids of finite length, the magnetic field lines do not lie wholly along the solenoidal axis as is generally assumed, and the exact orientation of the loop is not easily determined.

One can circumvent this difficulty by a convenient strategem. The voltage across an inductive circuit element containing negligibly small resistance is

$$V = L \frac{dI}{dt} . \qquad (1)$$

The ratio of the voltages across two such inductive elements in a series circuit is merely the ratio of the two inductances. Thus, if the capacitor bank is operated at sufficiently low energy so that the flyer plate does not move and the workpiece inductance remains constant, then

$$V_L = L_w \, dI/dt$$

for the voltage across the workpiece,

$$V_p = L_p \, dI/dt$$

for the loop voltage, and

$$\frac{V_p}{V_L} = \frac{L_p}{L_w} \qquad (2)$$

for the ratio of inductances, where L_w is the workpiece inductance. Then, if the workpiece inductance is known, one can determine the loop inductance simply from the voltage traces.

Before each test, the pickup loop was calibrated in this manner. In this particular experiment, the bank was first operated at 1.1 kilovolts, and traces of V_L and V_p were obtained. These traces are shown in Figures 12 and 13. Note that the two voltages are almost exactly in phase, indicating that the resistive voltage IR drop across the workpiece is

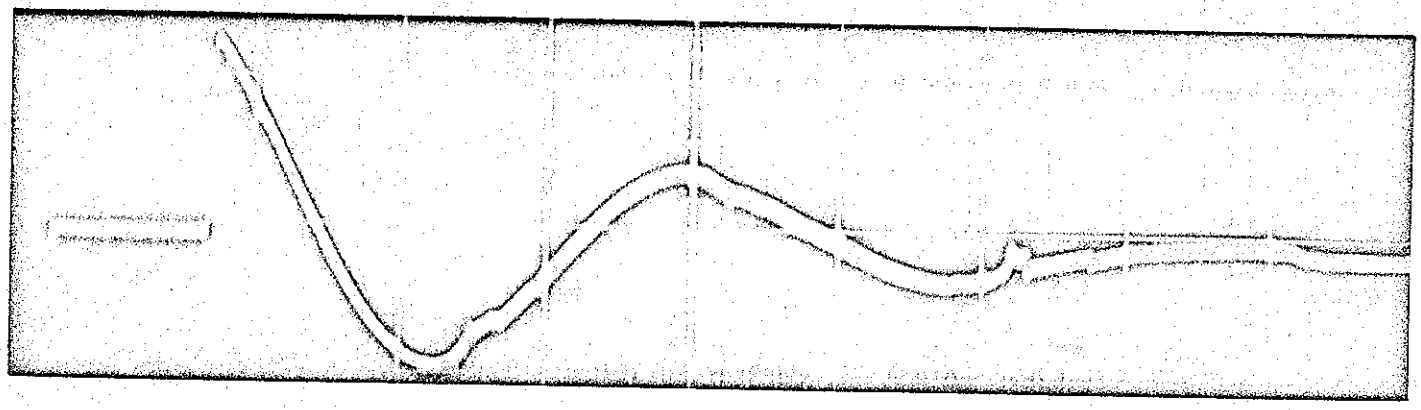

Figure 12. Calibration test loop voltage -- flat copper flyer plate experiment (5 volts per division; 10 microseconds per division).

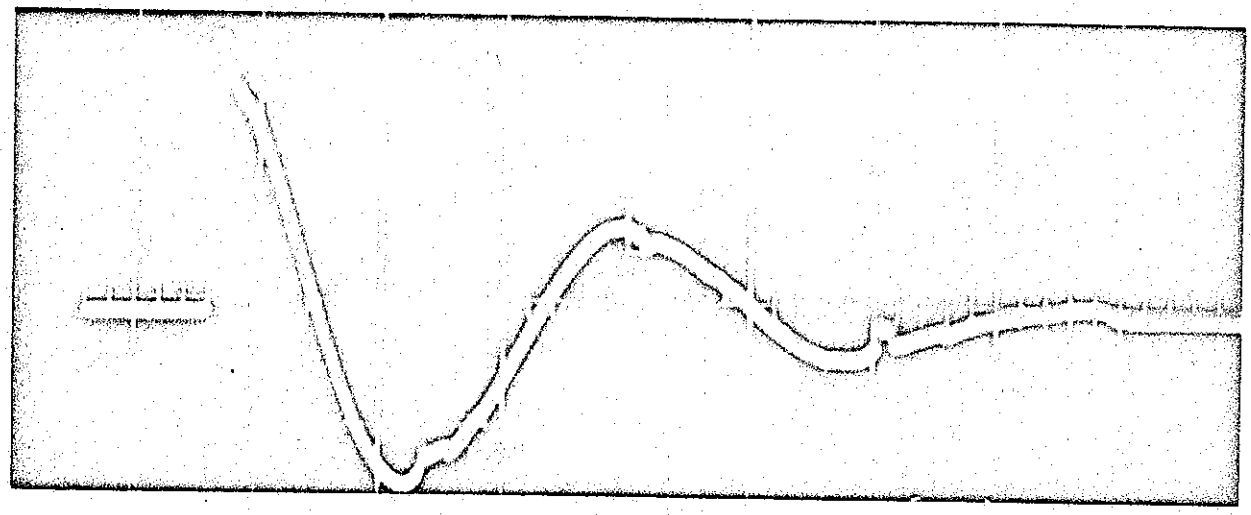

Figure 13. Calibration test load voltage -- flat copper flyer plate experiment (50 volts per division; 10 microseconds per division).

EG&G INC.

negligible compared with the inductive voltage $L_w dI/dt$. Both traces exhibit a ringing period of 35.8 microseconds. Comparison of the ratio of the voltages at successive maxima yields

At t = 0 $\quad \frac{V_L}{V_p} = 14.0$.

After one half-cycle $\quad \frac{V_L}{V_p} = 13.8$.

After one full-cycle $\quad \frac{V_L}{V_p} = 13.9$.

After three half-cycles $\quad \frac{V_L}{V_p} = 13.5$.

These four ratios are in agreement to within less than four percent. Choosing the average value,

$$L_p = \frac{L_w}{13.8} \quad . \tag{3}$$

The load inductance can be obtained directly from simple geometrical considerations. From conservation of energy requirements, one can show that this inductance is[5]

$$L_w = 4\pi \frac{A_{gap}}{\ell} \text{ nH} \tag{4}$$

where A_{gap} is the cross-sectional area in square centimeters of the insulating gap between the inner wall of the flux concentrator and the nearest metal surfaces of the workpiece, and ℓ is the length of the workpiece in centimeters.

The test sample consisted of an aluminum cylinder, originally 2.947 inches in diameter and cut flat on one side to a transverse dimension of 1.975 inches. Surrounding the aluminum sample was a strip of copper 10 mils in thickness, uniformly separated from the curved portion of the aluminum by 2 mils of mylar and then bent into a flat section parallel to the flat of the aluminum and separated from it by a distance of 0.625 inch. A cross sectional view of the entire workpiece is shown in Figure 14. The area of the insulating gap is

$$A_{gap} = \pi R_c^2 - \pi \times \frac{4.92}{2\pi} b^2 - 2.316 R_f \ cm^2 \qquad (5)$$

where R_c is the inner radius of the single-turn flux concentrator, b is the radius of the curved copper section and R_f is the perpendicular distance of the flat copper flyer plate from the center of the system. The curved section extends over 4.92 radians of arc.

From Equation (5) the inductance of the workpiece becomes

$$L_w = \frac{4\pi}{\ell} (\pi R_c^2 - 2.46 b^2 - 2.316 R_f) \ nH \qquad (6)$$

and for

R_c = 1.5075 inches = 3.829 centimeters

b = 1.4855 inches = 3.773 centimeters

R_f = 1.127 inches = 2.864 centimeters

ℓ = 2.853 inches = 7.247 centimeters

A_{gap} = 4.42 square centimeters and L_w = 7.7 nanohenries.

Thus, from Equation (3) the loop inductance becomes

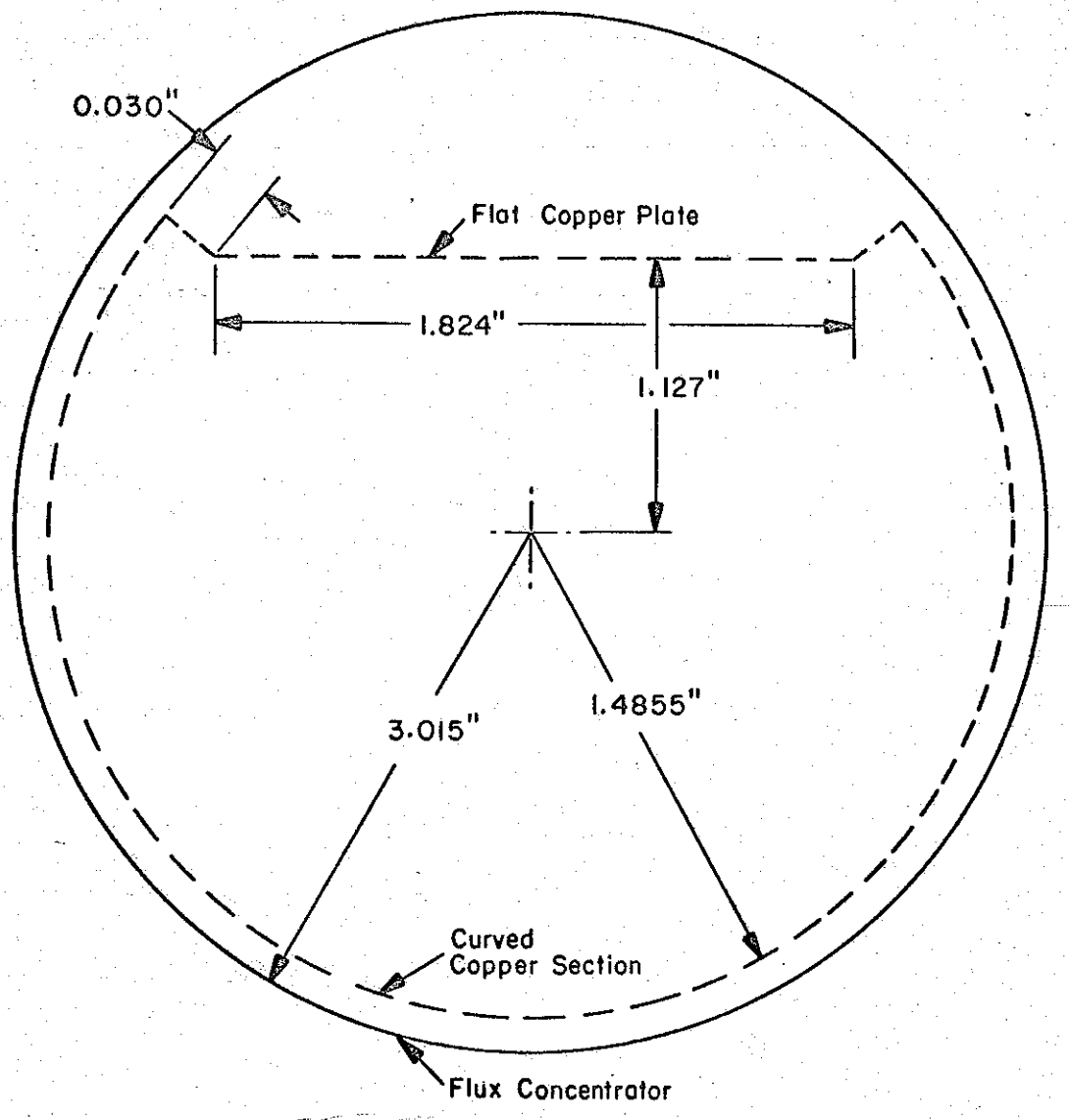

Figure 14. Cross-sectional view of workpiece -- flat copper flyer plate experiment.

$$L_p = \frac{L_w}{13.8} = 0.56 \text{ nH} .$$

This value of L_p is the calibration factor that enables one to directly convert the measured loop voltage, V_p, to the actual time rate of change of current. Once dI/dt has been so determined, the actual current is obtained by numerical integration methods.

Additional useful information is derivable from the calibration test. The period and profile of the voltage traces enable one to calculate the bank-ringing frequency and damping rate. As stated previously, the bank is operated at low voltages (approximately one kilovolt) during the calibration test so as not to deform the flyer plate and thus change the workpiece inductance. Then for a constant LRC circuit, one has for the current in a ringing circuit

$$I = I_o e^{-at} \sin\omega t$$

and

$$V = L\frac{dI}{dt} \alpha e^{-at} (\omega\cos\omega t - a \sin\omega t) \qquad (7)$$

where a is the damping rate in inverse seconds and $\omega = 2\pi f$ is the angular frequency.

If V_1 represents the voltage at time t, and V_2 the corresponding value at a time t_2 exactly one period later, then from Equation (7)

$$\frac{V_1}{V_2} = e^{+a\tau}$$

or

$$a = \frac{1}{\tau} \ln \frac{V_1}{V_2} \qquad (8)$$

where τ is the time of one period.

Calculating the ratio V_1/V_2 from either of the two voltage traces leads to an average value of

$$\frac{V_1}{V_2} = 3.15$$

and, thus, for $\tau = 35.8$ microseconds

$$a = 3.2 \times 10^4 \text{ sec}^{-1} .$$

The angular-ringing frequency is obtained directly from the period

$$\omega = \frac{2\pi}{\tau} = 1.75 \times 10^5 \text{ sec}^{-1} .$$

With ω and a both known, the total inductance of the circuit can be readily determined. The angular frequency of a ringing LRC circuit is related to the circuit elements by

$$\omega^2 = \frac{1}{LC} - a^2 . \qquad (9)$$

Solving this last result for the total circuit inductance, L, one obtains for $C = 168\ \mu F$

$$L = 187 \text{ nanohenries}$$

which supports the earlier assertion that the inductance of the workpiece (7.7 nanohenries) comprises but a small fraction of the total inductance of the circuit.

4.1.2 Determination of the Current and Magnetic Pressure Impulse. During the actual experiment, the flat copper flyer plate,

set into motion by the action of the magnetic pressure pulse, traversed the intervening space and struck the aluminum test piece, leaving a slight indentation in the aluminum surface. This motion was photographed with a Kerr Cell camera having an interframe time of 20 microseconds. The resultant photographs were closely examined and revealed an estimated maximum average velocity of 2.6×10^4 cm/sec.

The two appropriate voltage traces are shown in Figures 15 and 16. Note that in contrast with the traces obtained for the calibration test, the two voltages are no longer in phase. The fact that the loop voltage, which is a measure of dI/dt, leads the load voltage, V_L, suggests that the latter has acquired a resistive component as the pickup loop is designed to detect only the induced voltage created by the time-varying magnetic field. Even through the workpiece is itself a low-resistance element (approximately 0.3 milliohm), the currents flowing in the coil are great enough to produce a resistive (IR) voltage drop comparable in magnitude with the inductive voltage $L_w \frac{dI}{dt}$. Values of V_L, V_p, and dI/dt are listed in Table 1.

The most important parameter than can be ascertained by such an analysis is the time-integrated magnetic pressure. This magnetic pressure impulse is a remarkably reliable indicator of the maximum velocity achieved by the flyer plate. Additionally, its time history illustrates the chronology of the impulsive loading.

The magnetic pressure impulse is derivable from the current, which in turn is obtained from dI/dt by numerical integration. Values of current, I, are listed in Table 2 below and are plotted in Figure 17. The maximum current of 820 kiloamps occurs at 7.5 microseconds. These values agree quite well with the theoretical results for a constant LRC circuit. The maximum current in such a circuit is given by Equation (10).[5]

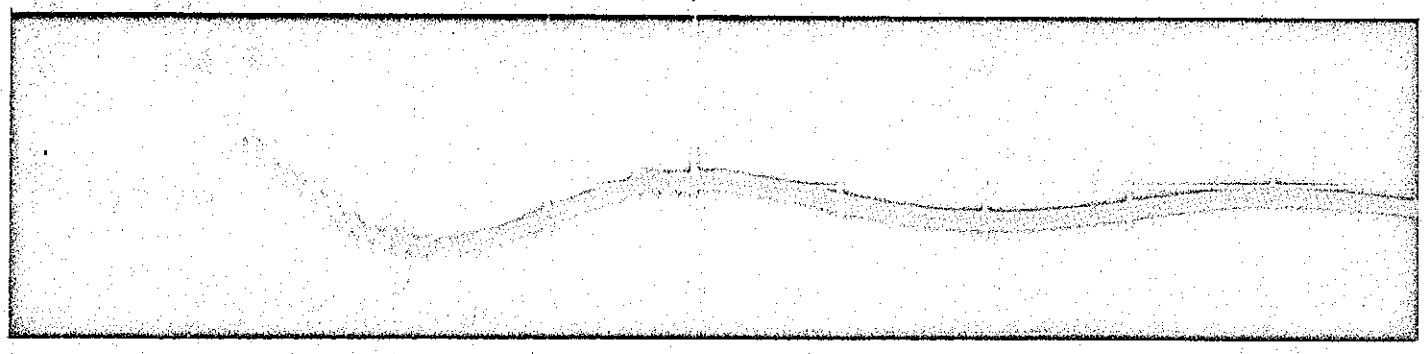

Figure 15. Loop voltage -- flat copper flyer plate experiment (200 volts per division; 10 microseconds per division).

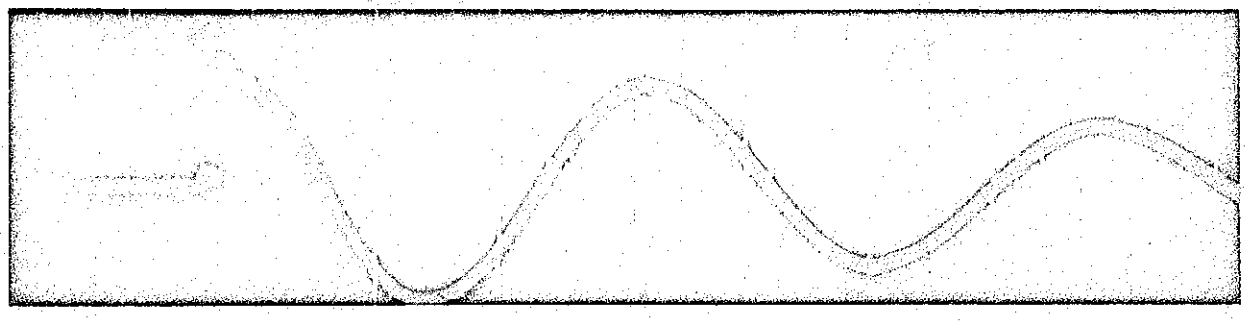

Figure 16. Load voltage -- flat copper flyer plate experiment (1.67 kilovolts per division; 10 microseconds per division).

AEGIS INC.

TABLE 1. VALUES RECORDED FROM VOLTAGE TRACES -- FLAT COPPER FLYER PLATE EXPERIMENT

time (μsec)	V_L (kV)	V_p (volts)	$\frac{dI}{dt}$ $\left(\frac{kA}{\mu sec}\right)$
0	1.81	120.8	220
1.0	1.70	116.6	212
2.0	1.48	99.3	181
3.0	1.38	68.5	125
4.0	1.26	44.2	80
5.0	1.13	30.6	56
6.0	0.96	15.5	28
7.0	0.74	5.4	10
8.0	0.46	-7.2	-13
9.0	0.12	-24.8	-45
10.0	-0.24	-39.4	-72
11.0	-0.53	-48.2	-88
12.0	-0.79	-52.8	-96
13.0	-1.05	-56.3	-102
14.0	-1.21	-64.3	-117
15.0	-1.39	-63.2	-115
16.0	-1.48	-60.1	-109
17.0	-1.50	-56.6	-103
18.0	-1.48	-52.0	-95
19.0	-1.43	-47.0	-85
20.0	-1.36	-42.0	-76

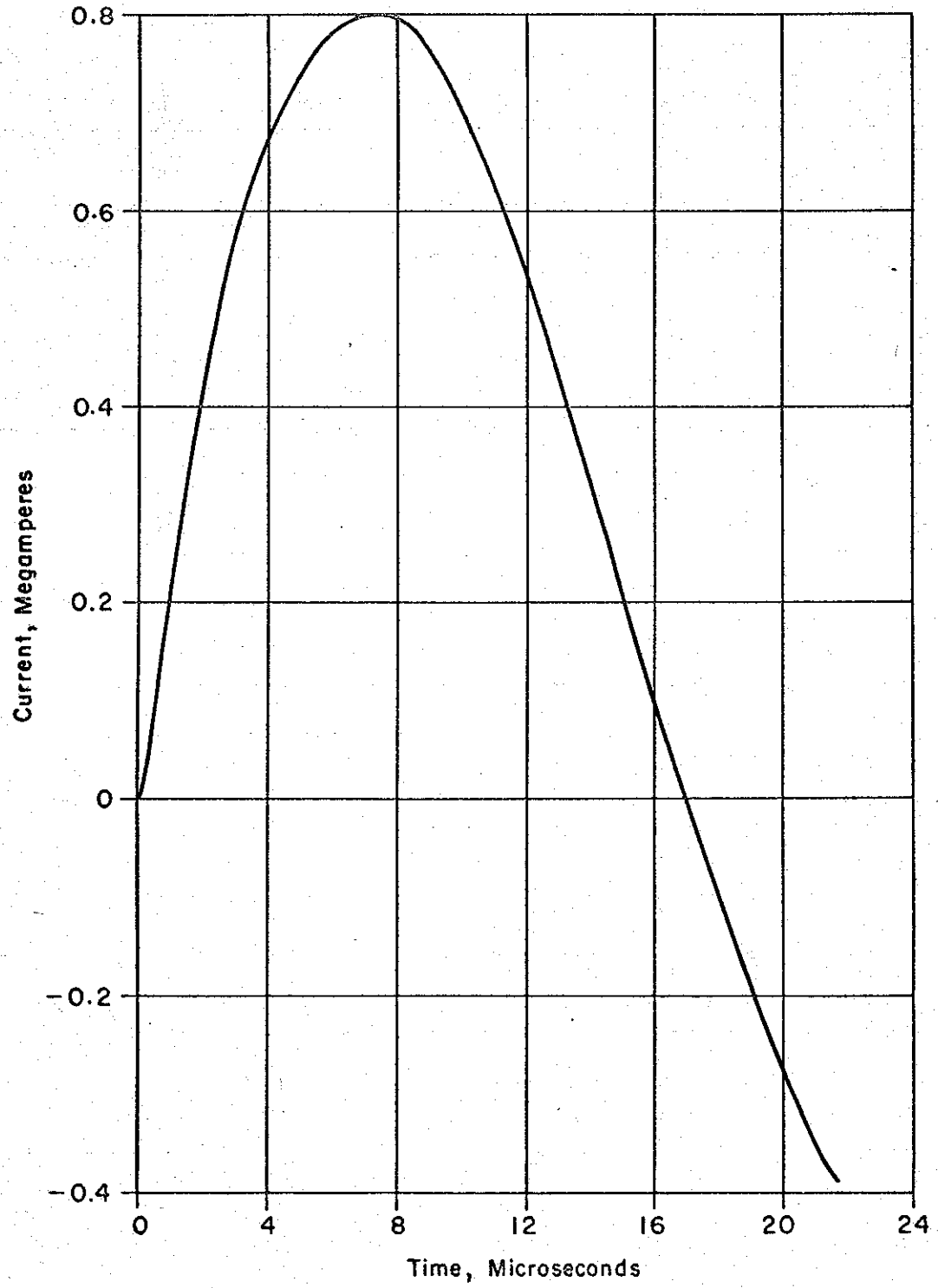

Figure 17. Current through workpiece -- flat copper flyer plate experiment.

$$I_{max} = 2 V_o \sqrt{\frac{C}{L}} e^{-at_{max}} \quad (10)$$

where

$$t_{max} = \frac{1}{\omega} \tan^{-1} \frac{\omega}{a} \quad (11)$$

and the factor of two appearing in Equation (10) represents the turns ratio of the windings.

Solving Equations (10) and (11) where $\omega = 1.75 \times 10^5$ sec^{-1}, $a = 3.2 \times 10^4$ sec^{-1}, $V_o = 19.4$ kV, $L = 187$ nH, and $C = 168$ μF, one obtains $t_{max} = 7.9$ μsec and $I_{max} = 890$ kA.

TABLE 2. CURRENT THROUGH THE WORKPIECE

time (μsec)	I (kA)	time (μsec)	I (kA)
0	0	11	629
1	220	12	537
2	414	13	438
3	573	14	328
4	671	15	211
5	739	16	99
6	781	17	-8
7	800	18	-107
8	797	19	-197
9	768	20	-277
10	709		

The magnetic field associated with this current gives rise to a magnetic pressure that is everywhere normally incident to the copper in the workpiece and of magnitude

$$P = \frac{2\pi}{\ell^2} I^2 \times 10^{-8} \quad \text{bars} . \tag{12}$$

The magnetic pressure is plotted in Figure 18. The peak magnetic pressure of 0.77 kilobar is achieved after 7.5 microseconds.

Numerical integration of the magnetic pressure yields the aforementioned impulse, which is plotted in Figure 19. Note that scant additional loading occurs after 14 microseconds.

Conservation of linear momentum allows one to relate this impulse directly to the velocity of the flyer plate. Once instabilities in the metal occur, momentum is not conserved, and this relationship is no longer valid. Prior to the onset of instabilities, one can equate the impulse to the momentum per unit area of the flyer plate. Thus,

$$\Gamma = \text{impulse} = mv_f \tag{13}$$

where $m = \rho h$ is the mass per unit area of the flyer and where h is the thickness of the copper. The Kerr Cell photographs show no instabilities prior to 20 microseconds. Choosing $t = 20$ microseconds, one finds from Figure 19

$$\Gamma = 6.74 \text{ millibar-sec}$$
$$= 6.74 \times 10^3 \frac{\text{dyne-sec}}{\text{cm}^2} .$$

Since $m = 2.25 \times 10^{-1}$ gm/cm^2, one obtains from Equation (13)

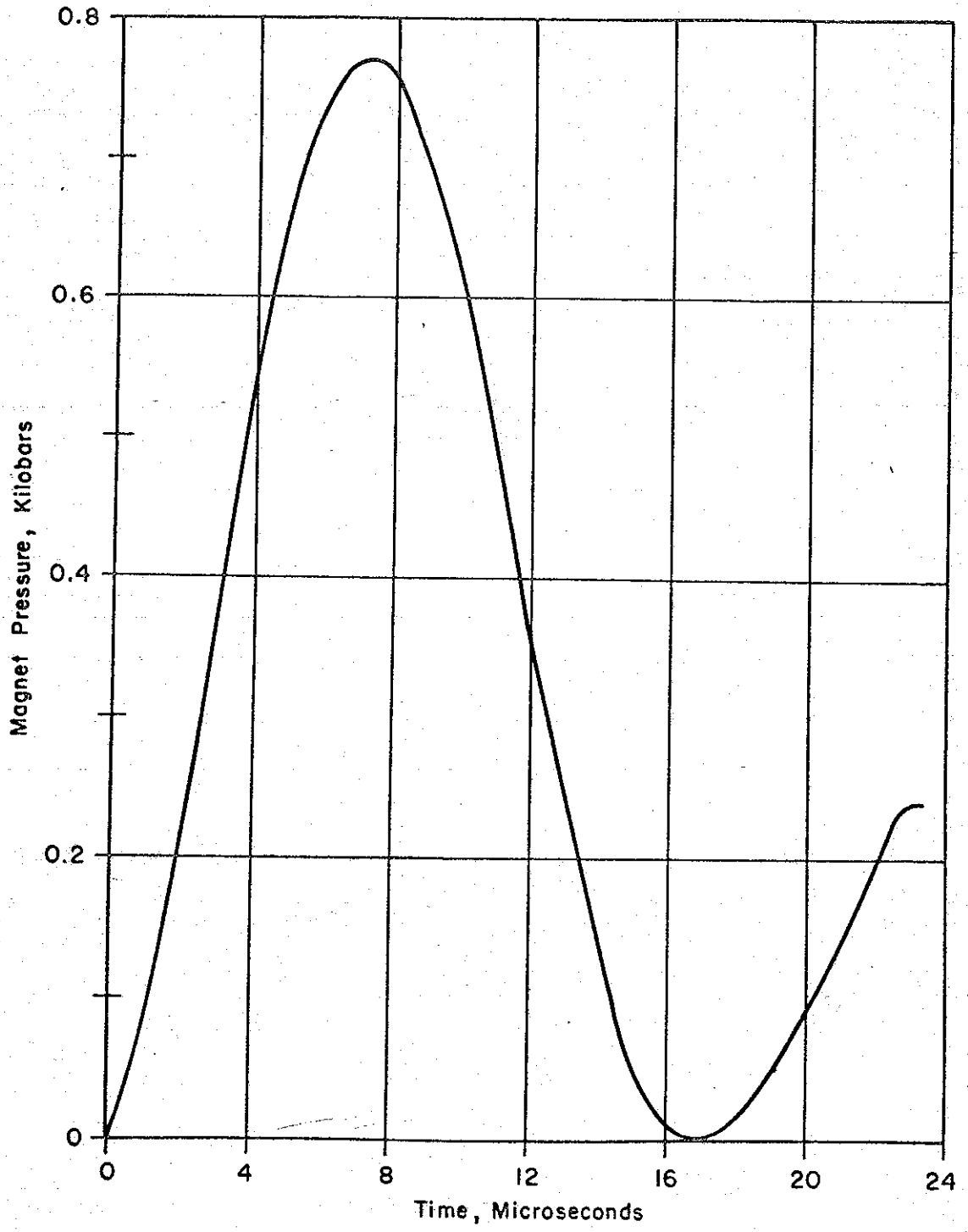

Figure 18. Magnetic pressure incident on flyer plate -- flat copper flyer plate experiment.

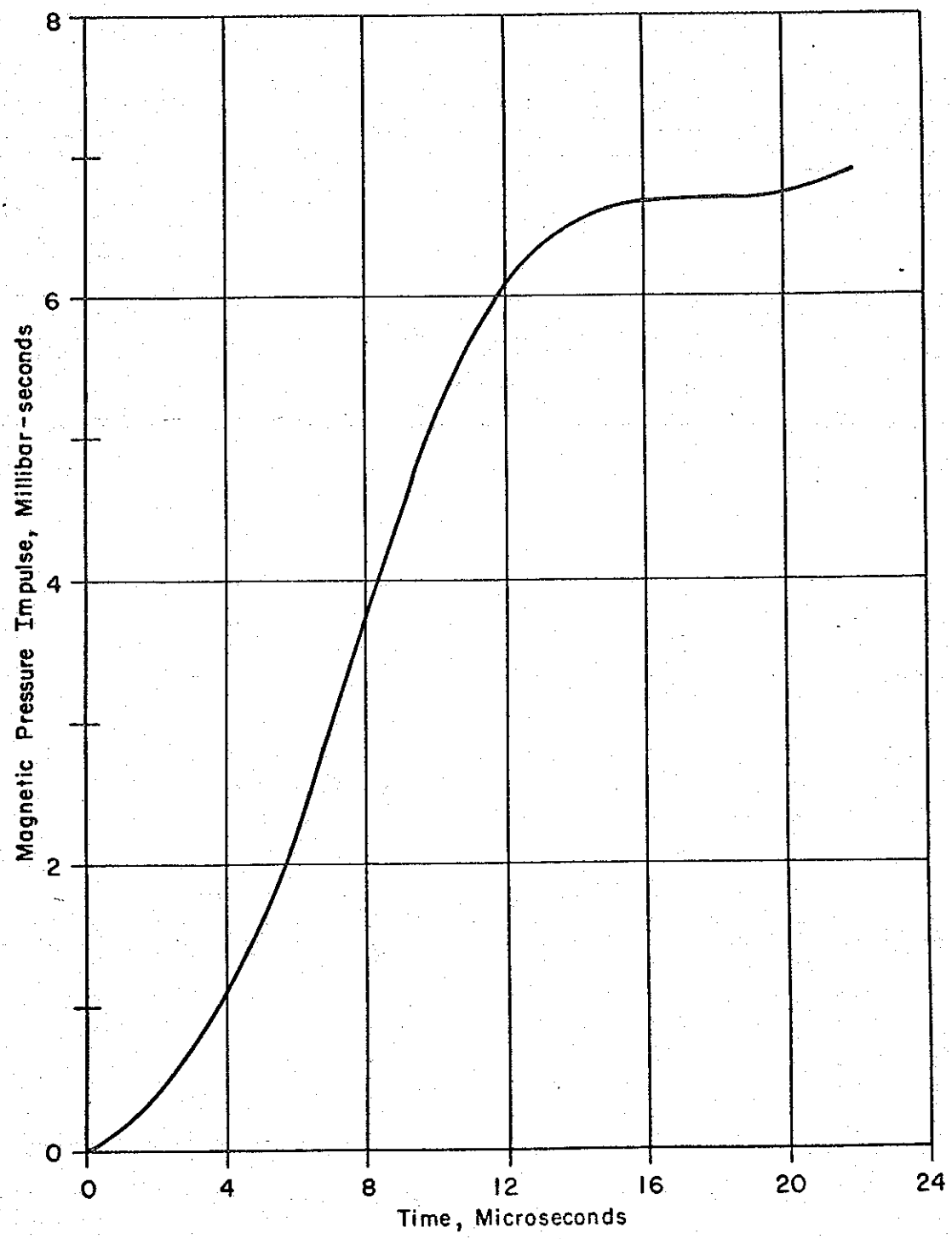

Figure 19. Magnetic pressure impulse -- flat copper flyer plate experiment.

$$v_f = 3 \times 10^4 \text{ cm/sec}$$

which is in excellent agreement with the value of 2.6×10^4 estimated from the photographs.

4.1.3 Determination of the Time-Varying Inductance. It is also possible to obtain the detailed time history of the flyer-plate motion, if the flyer is the only section of the workpiece that moves under the action of the magnetic pressure pulse. If the position of the flyer is the only variable, then using Equation (6) the workpiece inductance can be written in the following form:

$$L_w = F(R_f) \quad . \tag{14}$$

Differentiating both sides of Equation (14),

$$\frac{dL_w}{dt} = \frac{dF}{dt} v_f \tag{15}$$

or, more explicitly, from Equation (6)

$$\frac{dL_w}{dt} = \frac{4\pi}{\ell} \times 2.316 \; v_f \quad . \tag{16}$$

The negative sign appears because the motion is inward in the direction of increasing inductance. Thus, the velocity of the flyer plate can be directly related to the time rate of change of the workpiece inductance. This latter quantity can be calculated from the voltage traces.[4]

The voltage across a circuit element having a time-varying inductance L_w and an internal resistance R_L is

$$V_L = \frac{d}{dt}(L_w I) + IR_L \quad . \tag{17}$$

Solving Equation (17) for the inductance,

$$L_w = \frac{1}{I}\int_o^t (V_L(t') - R_L I(t'))dt' = \frac{\Phi}{I} \tag{18}$$

where $\Phi = \int_o^t (V_L - IR_L)\, dt'$ is an integrated voltage.

The time derivative of L_w is obtained directly from Equation (18):

$$\frac{dL_w}{dt} = \frac{V_L - IR_L}{I} - \frac{\Phi}{I^2}\frac{dI}{dt} \quad . \tag{19}$$

These two results illustrate the significance of measuring V_L and dI/dt, for all the pertinent quantities needed to obtain L_w and its time derivative are contained in the two voltage traces.

The resistance of the workpiece can easily be computed. The flux concentrator, because of its large metallic cross section, possesses the minimal skin-depth resistance. Since the skin-depth of 20 mils is twice the thickness of the copper in the workpiece, the resistance of the flux concentrator is one-half the resistance of the copper. The resistance of the flat copper section is 0.04 milliohm, while the curved copper section, because of its greater current-path length, has a resistance of 0.16 milliohm. Thus, the total resistance of the copper is 0.2 milliohm, and the resistance of the entire workpiece is, accordingly, 0.3 milliohm.

Choosing R_L = 0.3 milliohm, one can readily determine V_L - IR, perform the necessary integration, and evaluate L_w. Values of the time-varying inductance are plotted in Figure 20. Over the first 20

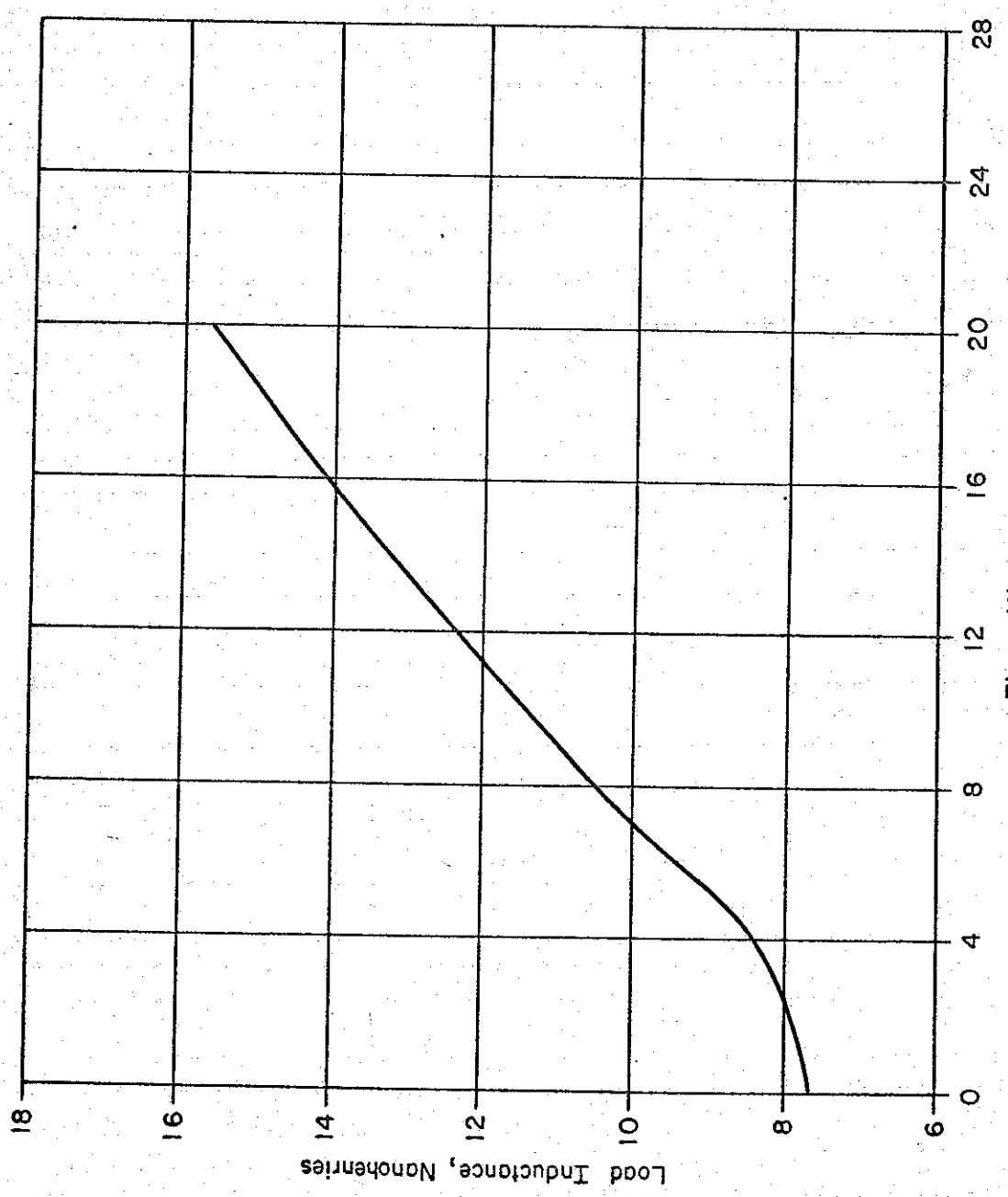

Figure 20. Time variation of workpiece inductance -- flat copper flyer plate experiment.

microseconds, L_w more than doubles its initial value of 7.7 nanohenries. The inductance does not change appreciably until the third microsecond and then increases by an average of 0.45 nanohenry over each successive microsecond.

Values of $\frac{dL_w}{dt}$ are listed below in Table 3. The maximum value of 0.57 nH/μsec occurs near the time of maximum current. This time rate of change of inductance is directly related to the velocity of the flyer plate if, and only if, the flat copper section alone moves under the action of the magnetic pressure. Unfortunately, the Kerr camera photographs showed motion on the part of the curved copper section, and an examination of the workpiece after completion of the test confirmed this observation.

Therefore, the radius of the curved section is also a variable, and Equations (14) and (15) are not true for this case. Future experiments will be designed so that only the flyer plate is set into motion during the test, and the velocity time profile of the flyer can then be obtained directly from the time-varying inductance.

4.1.4 Efficiency of the System. The efficiency of the capacitor-bank system, in doing work on the flyer plate, is of prime concern. Clearly, only that portion of the bank energy that is stored in the inductance of the workpiece is available for such a purpose. The maximum value of this inductively stored energy is

$$E_s^{max} = \frac{1}{2} L_w I_{max}^2 .$$

Since L_w is a small fraction of the total circuit inductance, variations in L_w do not greatly perturb the current in the circuit. Thus, one can approximate the actual conditions by a constant LRC circuit. The expression for the maximum stored energy can then be written for the

TABLE 3. TIME RATE OF CHANGE OF INDUCTANCE

time (μsec)	$\frac{dL}{dt}$ *
0	0.00
1	0.00
2	0.00
3	0.35
4	0.55
5	0.53
6	0.57
7	0.49
8	0.44
9	0.47
10	0.50
11	0.51
12	0.50
13	0.48
14	0.54
15	0.54
16	0.45
17	0.40
18	0.35
19	0.33
20	0.28

* $\frac{dL}{dt}$ is given in units of milliohms or nH/μsec, which are equivalent.

general case of a series circuit containing a load inductance L_w and a total circuit inductance L:

$$E_s^{max} = \frac{n^2 L_w}{L} \exp\left(-2\frac{a}{\omega}\tan^{-1}\frac{\omega}{a}\right)E_o \qquad (20)$$

where n is the turns ratio of the windings, and $E_o = \frac{1}{2}CV_o^2$ is the bank energy.

If all of this stored energy goes into moving the flyer plate, then the maximum efficiency of the system is

$$\eta_{max} = \frac{n^2 L_w}{L} \exp\left(-2\frac{a}{\omega}\tan^{-1}\frac{\omega}{a}\right) . \qquad (21)$$

For the actual experiment, L_w = 10 nanohenries at the time of current maximum, L ~ 189 nanohenries and n = 2. One thus obtains for the maximum efficiency

$$\eta_{max} = 11.5 \text{ percent}$$

The efficiency of such a system will always be low because of the relatively large bank inductance of 45 nanohenries.

One can also determine the actual work done on moving the copper. The work necessary to change the inductance of the workpiece is[4]

$$W_s = \frac{1}{2}\int_o^t \frac{dL_w}{dt'} I^2 \, dt' . \qquad (22)$$

Again performing the integration numerically, one obtains, after 20 microseconds,

$$W_s = 1.4 \text{ kilojoules.}$$

Since the total-bank energy is 31.4 kilojoules at 19.4 kilovolts, this represents an actual efficiency of only 4.5 percent.

It should be noted, however, that the flyer plate (mass 3.84 grams) moving with a velocity of 3.3×10^4 cm/sec has a kinetic energy of only 0.21 kilojoule. The kinetic energy required to achieve a final velocity of 10^5 cm/sec is not beyond the realm of capability of the present system.

4.2 SIMULATED COSINE LAW LOADING

In an attempt to simulate cosine law loading, the experimental geometry shown in Figure 11 was chosen. Although photographic evidence is clear that these attempts were not successful, a detailed analysis has been made of the electrical data as a guide to future efforts. It, of course, relates only to the motion of the copper workpiece and not to that of the dielectric materials. In the case here analyzed, the copper flat shown in Figure 11 was 1.5 inches wide. Under the magnetic field pressure, it drove a piece of hexcel 0.375 inch thick at the center. The cylindrical surface, whose radius of curvature was 1.8125 inches, was faced with a phenolic sheet 0.03125 inch thick. Otherwise the workpiece was as shown in Figure 11.

4.2.1 Calibration Tests. A calibration test, similar to that described in the preceding section, was conducted prior to the actual experiment. The two voltage traces are displayed in Figures 21 and 22. The ratio of these two in-phase voltages was found to have an average value of 11.3. Therefore, from Equation (2)

$$L_p = \frac{L_w}{11.3} .$$

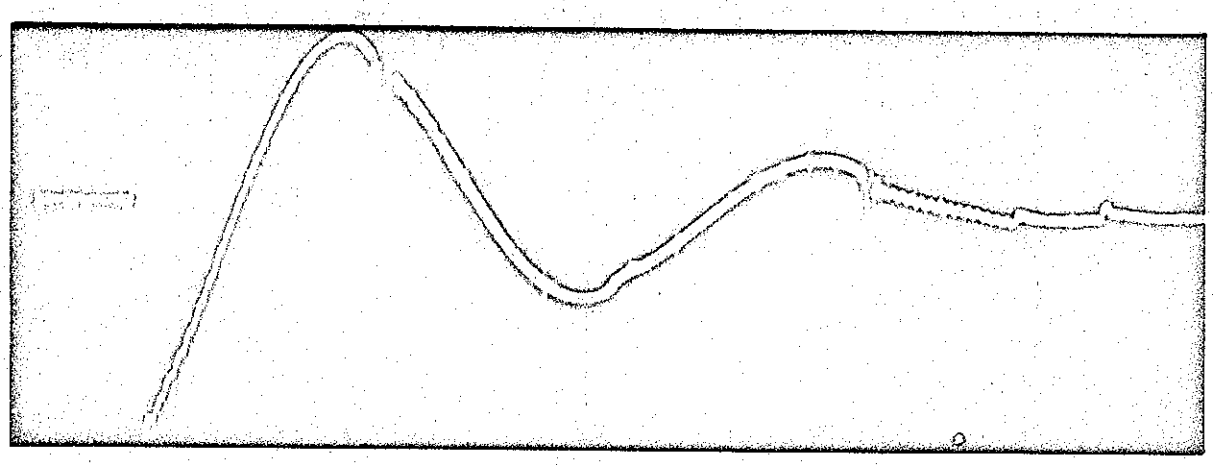

Figure 21. Calibration test loop voltage -- cosine loading experiment (5 volts per division; 10 microseconds per division).

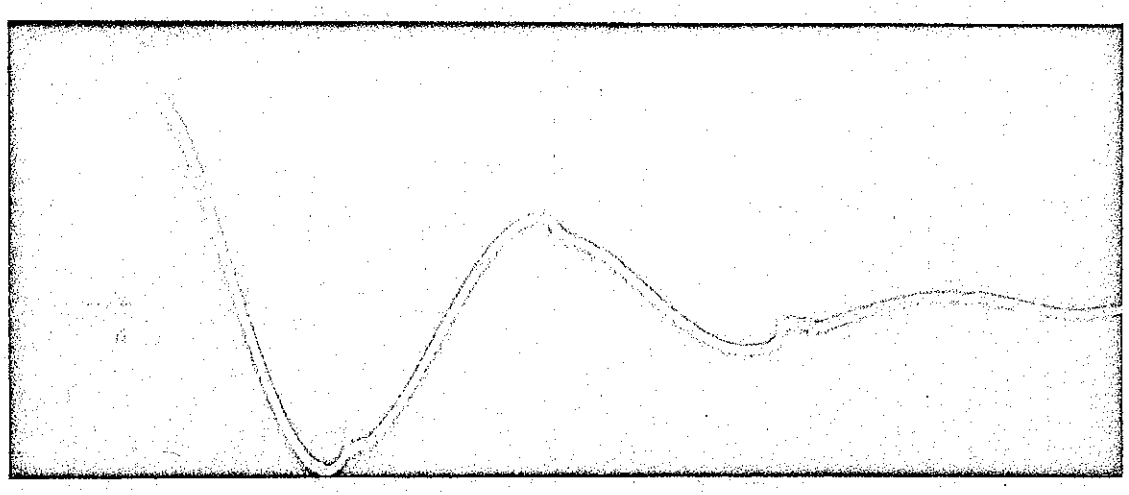

Figure 22. Calibration test load voltage -- cosine loading experiment (50 volts per division; 10 microseconds per division).

EG&G INC.

The workpiece inductance is determined from the area of the insulating gap between the inner surface of the flux concentrator and the nearest metal surfaces. One finds for the configuration shown in Figure 11

$$A_{gap} = 5.50 \text{ cm}^2 ,$$

From Equation (3) one then obtains for $\ell = 6.99$ centimeters (2.75 inches):

$$L_w = 10.4 \text{ nH}$$

and hence,

$$L_p = \frac{L_w}{11.3} = 0.93 \text{ nH}$$

is the proper calibration factor.

From the voltage traces, the length of one period was measured to be 35.9 microseconds, which corresponds to an angular-ringing frequency of $1.75 \times 10^5 \text{ sec}^{-1}$.

4.2.2 Determination of the Current and Magnetic Pressure Impulse. Kerr Cell photographs, taken during the actual test, indicated that the copper portion of the flyer plate had moved through the lower density hexcel, rather than the entire structure, having been uniformly accelerated toward the test cylinder.

The two voltage traces are shown in Figures 23 and 24. The initial load voltage provides an alternate method of determining the workpiece inductance prior to deformation. At $t = 0$, the ratio of the load voltage to the total bank voltage, V_o, must equal the ratio of twice the workpiece inductance to the total inductance of the circuit; i.e.,

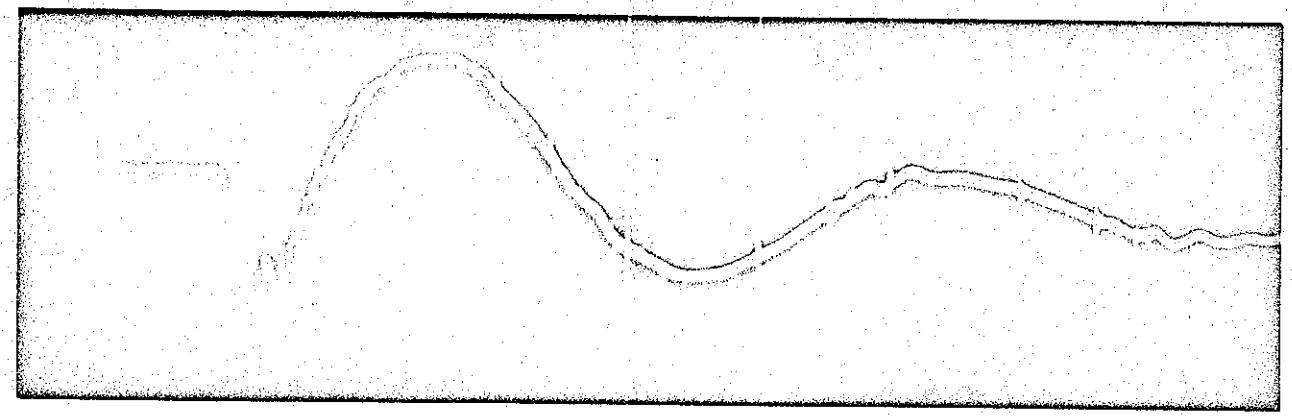

Figure 23. Loop voltage -- cosine loading experiment (100 volts per division; 10 microseconds per division).

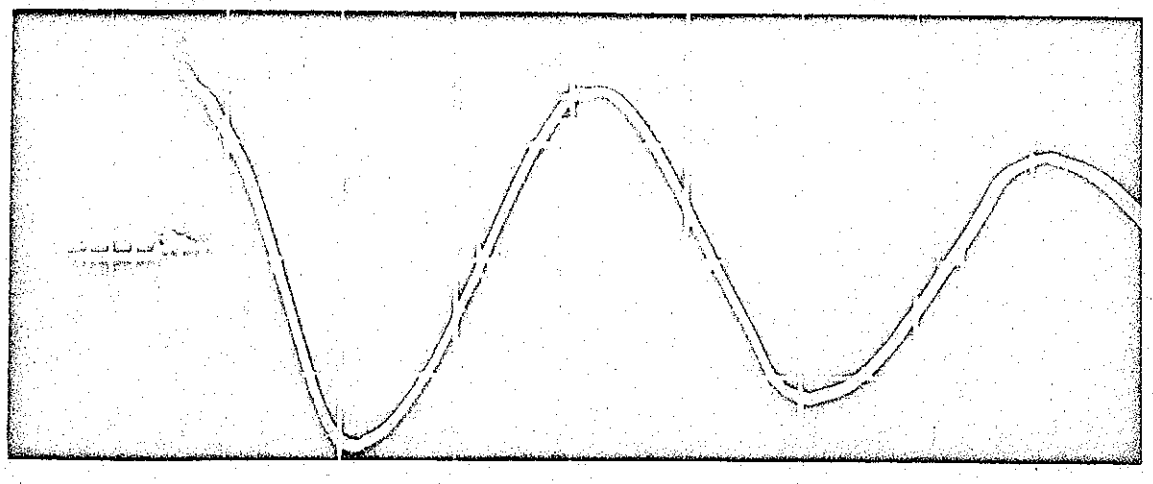

Figure 24. Load voltage -- cosine loading experiment (1 kilovolt per division; 10 microseconds per division).

EG&G INC.

$$\frac{V_L\ (t=0)}{V_o} = \frac{2L_w}{L} \qquad (23)$$

where the factor of two again represents the turns ratio of the windings. The bank was again discharged at 19.4 kilovolts and the initial value of the load voltage was observed to be 2.10 kilovolts.

The total circuit inductance is 190 nanohenries, as determined from the calibration test. One, thus, obtains, for the inductance of the workpiece, L_w = 10.3 nanohenries which agrees quite well with the value of 10.4 nanohenries calculated from the area of the insulation gap.

Values of load voltages and dI/dt are listed in Table 4. Again, one can readily observe that these two voltages are no longer in phase, the latter again leading the former. This again suggests the presence of a resistive IR voltage drop, which cannot be neglected with respect to the inductive or reactive voltage, L_w dI/dt.

The current is obtained from dI/dt by numerical integration and is plotted in Figure 25. The current has a maximum value of 710 kiloamps, which again occurs at 7.5 microseconds. These values agree closely with the current in a constant LRC circuit having equivalent circuit parameters.

The magnetic pressure is again simply determined from the current by the relationship

$$P = \frac{2\pi}{\ell^2} I^2 \times 10^{-8} \quad \text{bars} \qquad (24)$$

and has a maximum value of 0.64 kilobar at the time of current maximum. The magnetic pressure is plotted in Figure 26. The magnetic pressure impulse is then obtained by numerical integration and is plotted as a function

TABLE 4. VALUES RECORDED FROM VOLTAGE TRACES -- COSINE LOADING EXPERIMENT

time (μsec)	V_L (kV)	$\frac{dI}{dt}$ $\left(\frac{kA}{\mu sec}\right)$
0	2.10	196
1	1.95	180
2	1.66	146
3	1.47	99
4	1.38	76
5	1.21	38
6	1.06	29
7	0.87	3
8	0.64	-17
9	0.35	-32
10	0.04	-55
11	-0.28	-68
12	-0.63	-74
13	-0.94	-85
14	-1.24	-89
15	-1.46	-92
16	-1.59	-93
17	-1.62	-92
18	-1.58	-88
19	-1.54	-83
20	-1.45	-71
21	-1.33	-62
22	-1.19	-52
23	-1.04	-39
24	-0.87	-24
25	-0.68	-9
26	-0.45	7
27	-0.24	18
28	-0.02	29
29	+0.21	44
30	0.44	55

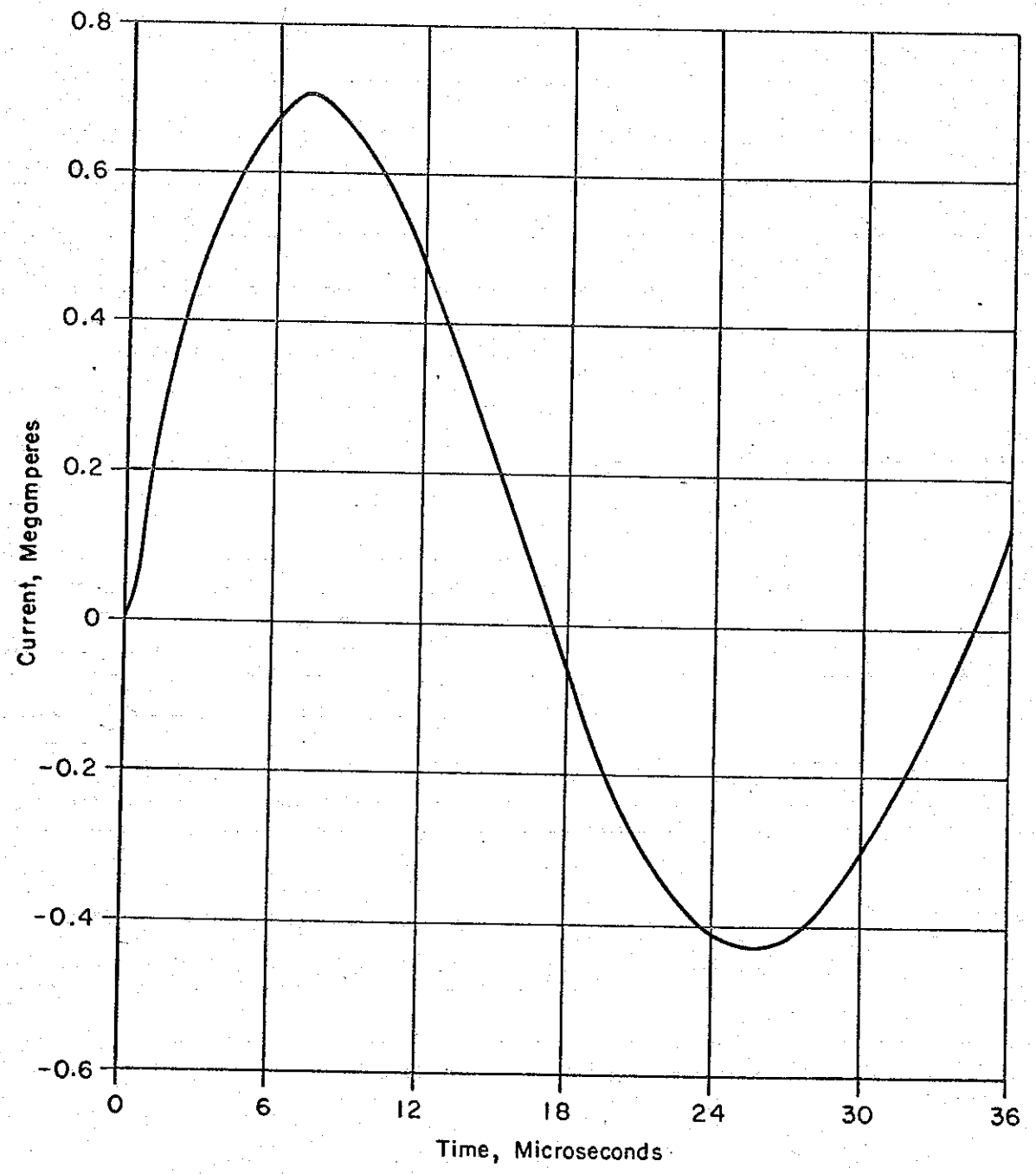

Figure 25. Current through workpiece -- cosine loading experiment.

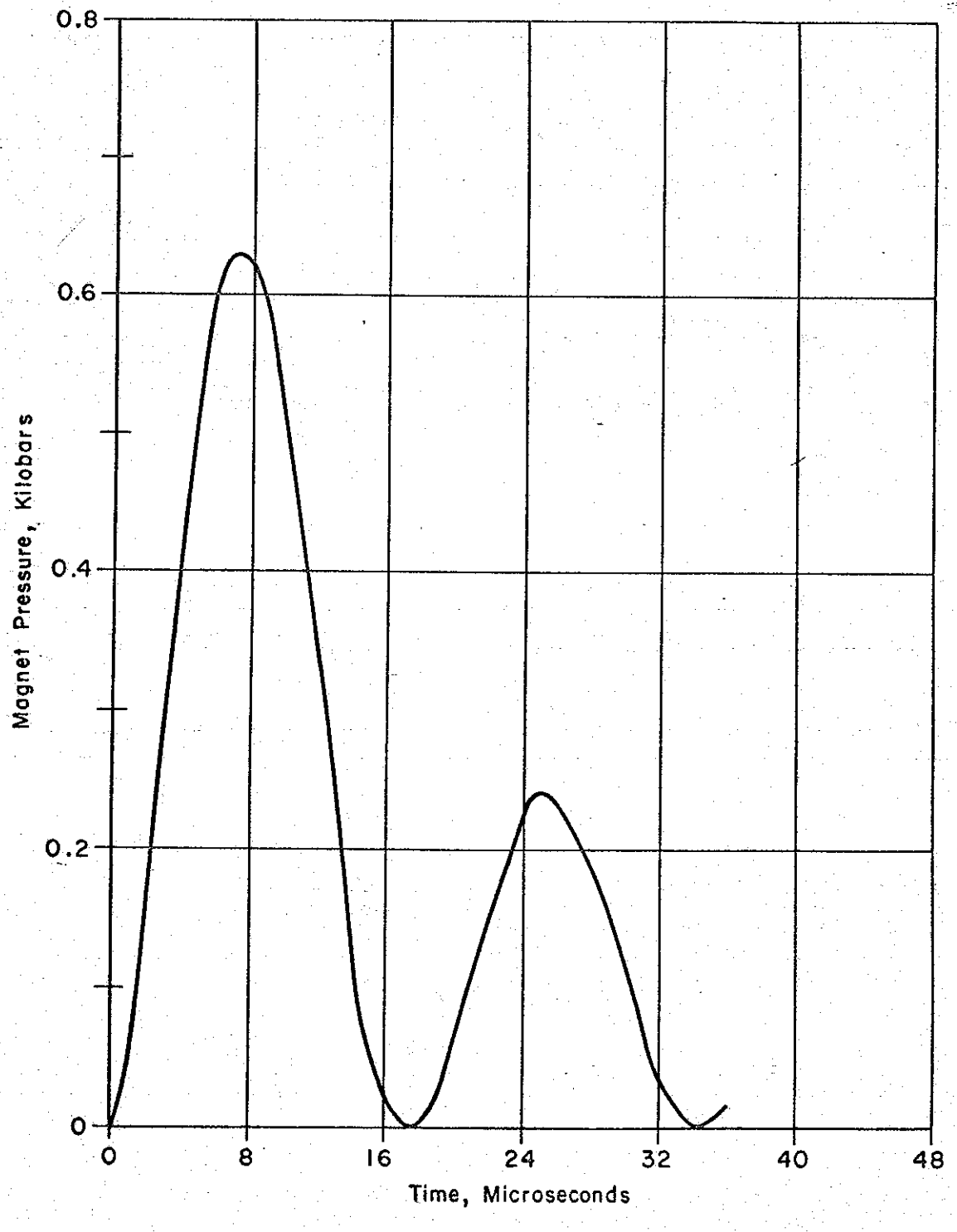

Figure 26. Magnetic pressure incident on flyer plate -- cosine loading experiment.

of time in Figure 27. This plot also illustrates the shape of the loading curve. Note that little additional loading occurs after 30 microseconds.

Again, in the absence of buckling or other instabilities, application of the conservation of momentum allows one to relate the magnetic pressure impulse to the velocity of the flyer plate according to the prescription

$$\Gamma = mv_f \quad .$$

The mass per unit area is comprised of three terms:

$$m = \rho_c h_c + \rho_H h_H + \rho_p h_p \qquad (25)$$

where ρ and h are the respective densities and thicknesses of the three materials: copper, hexcel, and phenolic. The center of mass of the hexcel is located along its center line at a distance of 0.57 centimeter (0.22 inch) from its outer boundary. Thus, $h_H = 1.14$ centimeters.

For

$$\rho_c = 8.95 \text{ gm/cm}^3,$$

$$\rho_H = 0.065 \text{ gm/cm}^3,$$

$$\rho_p = 1.35 \text{ gm/cm}^3,$$

$$h_c = 2.54 \times 10^{-2} \text{ cm},$$

$$h_H = 1.14 \text{ cm, and}$$

$$h_p = 7.94 \times 10^{-2} \text{ cm},$$

$$m = 0.373 \text{ gm/cm}^2 \quad .$$

Since the magnetic pressure impulse has a value of $7.4 \times 10^3 \ \frac{\text{dyne-sec}}{\text{cm}^2}$ after one cycle, the velocity from Equation (25) becomes

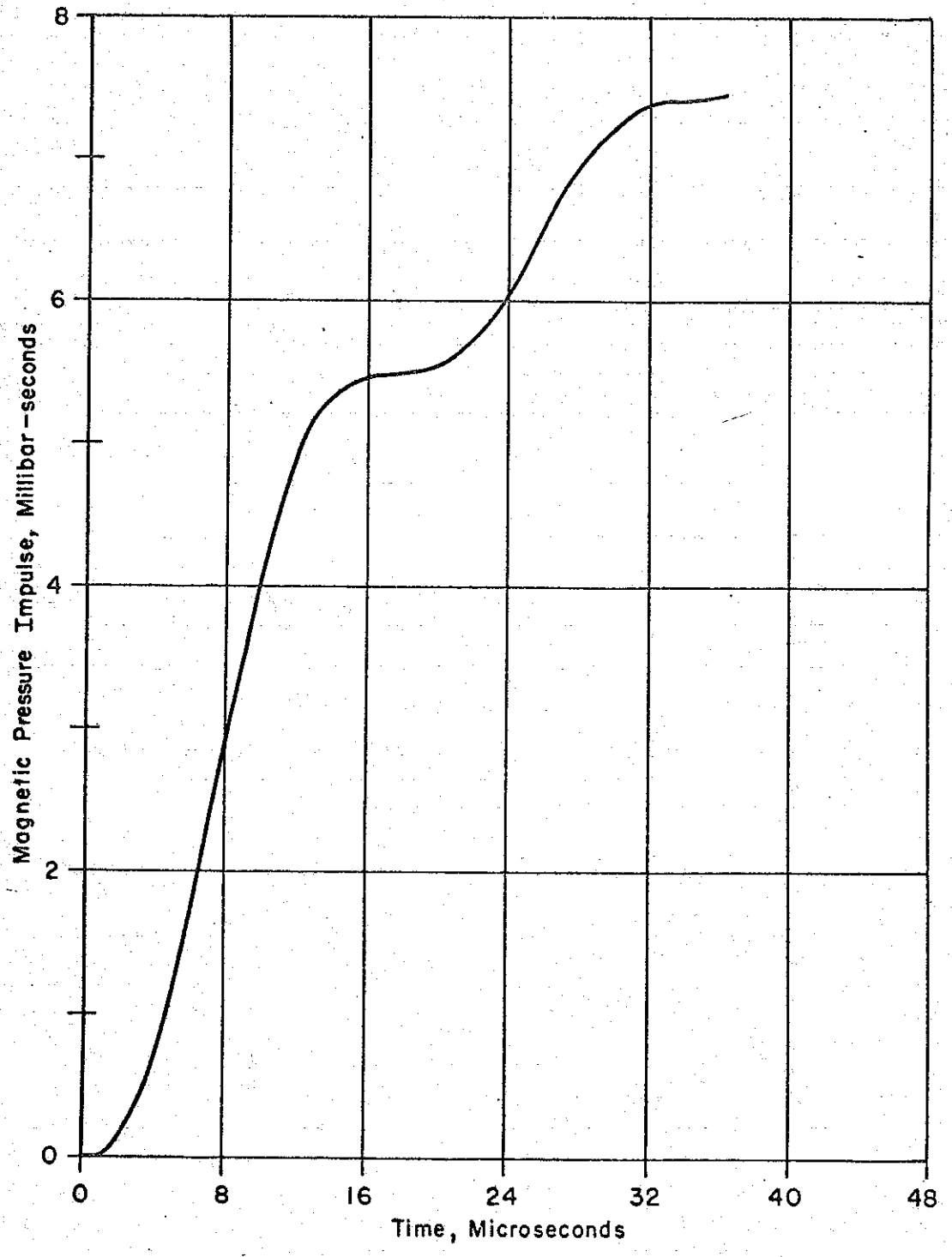

Figure 27. Magnetic pressure impulse - cosine loading experiment.

$$v_f = \frac{\Gamma}{m} = 2 \times 10^4 \text{ cm/sec} .$$

4.2.3 Determination of the Time-Varying Inductance. The inductance, $L_w(t)$, and its time derivative are both determined in the manner described in Section 4.1.3. The inductance is simply the ratio of the integrated voltage, Φ, to the current, I. All of the information needed is contained in the two voltage traces, except the workpiece resistance, R_L. The resistance of the flux concentrator was previously calculated to be 0.1 milliohm. The 240-degree curved copper section has a resistance of 0.3 milliohm, while the resistance of the copper flyer plate is 0.1 milliohm. The total resistance of the workpiece is, therefore, 0.5 milliohm. With R_L known, the inductance is again

$$L_w = \int_0^t \frac{(V_L - IR_L)\, dt}{I} = \frac{\Phi}{I} . \qquad (26)$$

If one does not subtract the resistive voltage IR drop from the measured value of V_L, the resulting integrated voltage will not be in phase with the current. Then, at some point in time the inductance, as calculated from Equation (26), will have a negative value, which is clearly impossible from a physical viewpoint.

Values of the time-varying inductance are plotted in Figure 28. A maximum $\frac{dL_w}{dt}$ of 1.3 milliohms (nH/μsec) occurs between 6 and 14 microseconds. Once again, the time rate of change of L_w cannot be related to the velocity of the flyer plate because the curved section of copper is also observed to move during the course of the experiment. In fact, the magnetic pressures produced are sufficient to even slightly deform the steel test cylinder.

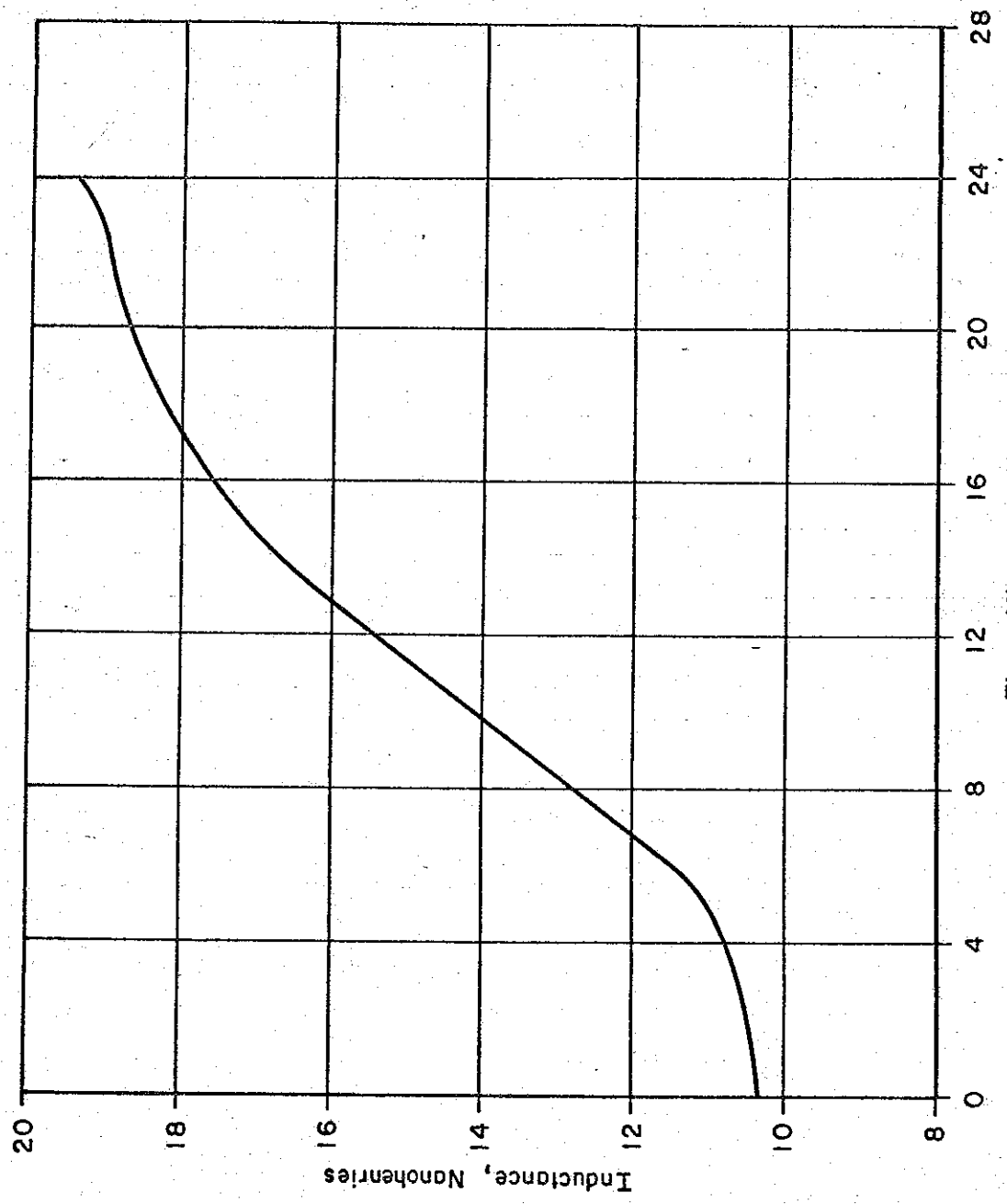

Figure 28. Time variation of workpiece inductance -- cosine loading experiment.

4.2.4 Efficiency of the System. The maximum theoretical efficiency of the system is computed in the same manner as in Section 4.1.4.

This efficiency represents the fraction of the total bank energy that can be stored in the magnetic field of the workpiece. The inductance of the workpiece is 12.5 nanohenries at the time of current maximum, whereas the total circuit inductance is 192 nanohenries at that time. For the same damping rate and angular frequency determined in Section 4.1, one finds η_{max} = 13 percent.

A direct calculation of the work done in changing the inductance of the workpiece by evaluating the integral

$$W_s = \frac{1}{2} \int_o^t \frac{dL_w}{dt'} I^2 \, dt'$$

yields a value of

$$W_s = 2.2 \text{ kilojoules.}$$

Since the total bank energy is 31.4 kilojoules at 19.4 kilovolts, this represents an actual efficiency of 7 percent.

On the other hand, the kinetic energy of the flyer plate, moving at a velocity of 2×10^4 cm/sec, is much less than 2.2 kilojoules. As was previously shown, the complete flyer plate (copper, hexcel, and phenolic) has a per unit area mass of 0.37 gm/cm^2 and therefore a total mass of 10.0 grams, since it contains an average surface area of 27 square centimeters. The kinetic energy of the flyer is simply

$$K = \frac{1}{2} M v_f^2 = 2 \times 10^9 \text{ ergs} = 200 \text{ joules}$$

which represents only a small fraction of W_s. Again, the kinetic energy associated with a flyer plate velocity of 10^5 cm/sec does not lie far beyond the capability of the present system.

4.3 LARGE DIAMETER PHENOLIC FLYER PLATES

The experiments of this category are described in Section 3.2.2. As a preliminary to the following detailed analysis of the results of one of these experiments, it is interesting to note the limitations of the existing bank in attempting to provide impulsive loading over sectors of large cylinders. For the 7-inch OD, 9-inch long phenolic test cylinder, the maximum pressure attainable is approximately 0.06 kilobar, one order of magnitude less than that achieved earlier in shorter geometries. Advantage was quickly taken, therefore, of the inverse square relationship between pressure and flyer-plate length to achieve significant pressures with a 2-inch long flyer plate. Further improvements in geometry, to be discussed in Chapter 5, are expected to give even greater effects. The following analysis pertains to flyer plate and test sample length of 2 inches in the geometry of Figure 7.

4.3.1 Calibration Tests. The dI/dt data was gained from a square pickup loop oriented in the central plane of the coil as indicated in Figure 7. The load voltage was measured at points as close as practicable to the inside ends of the coil air gap.

The calibration tests were again conducted at a low voltage (0.9 kilovolt). Examination of the two voltage traces, Figures 29 and 30, revealed a shorter period, and increased frequency, due to the absence of the added inductance of the multiple-turn coil. The period was measured to be 20.8 microseconds, considerably less than the 36-microsecond periods obtaind with the multiple-turn coil. This 20.8-microsecond period

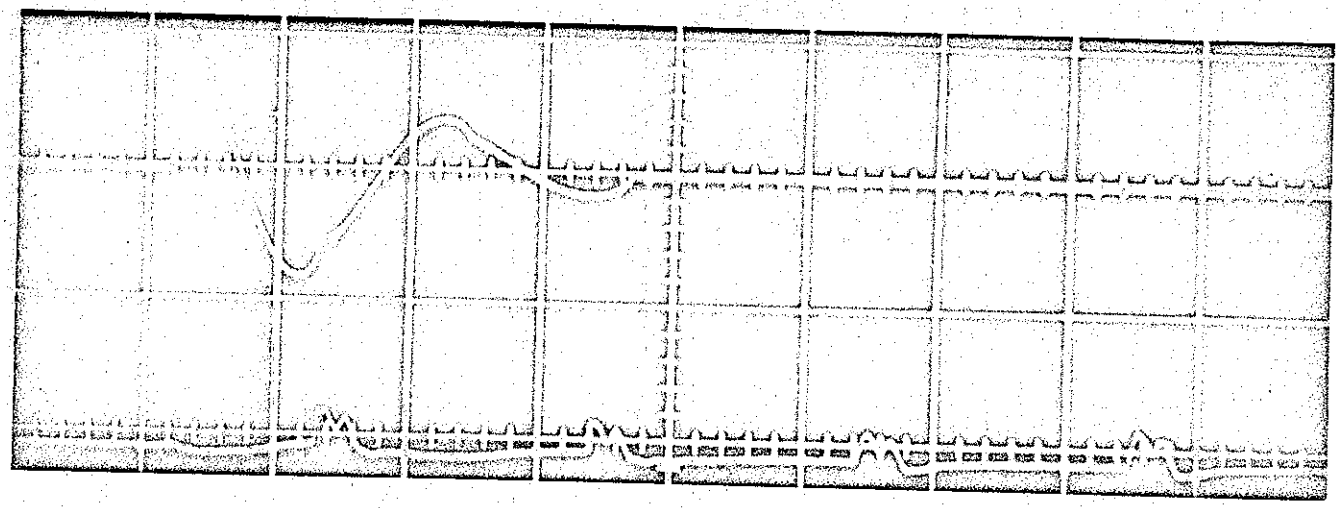

Figure 29. Calibration test loop voltage -- large diameter phenolic flyer plate experiment (5 volts per division; 10 microseconds per division).

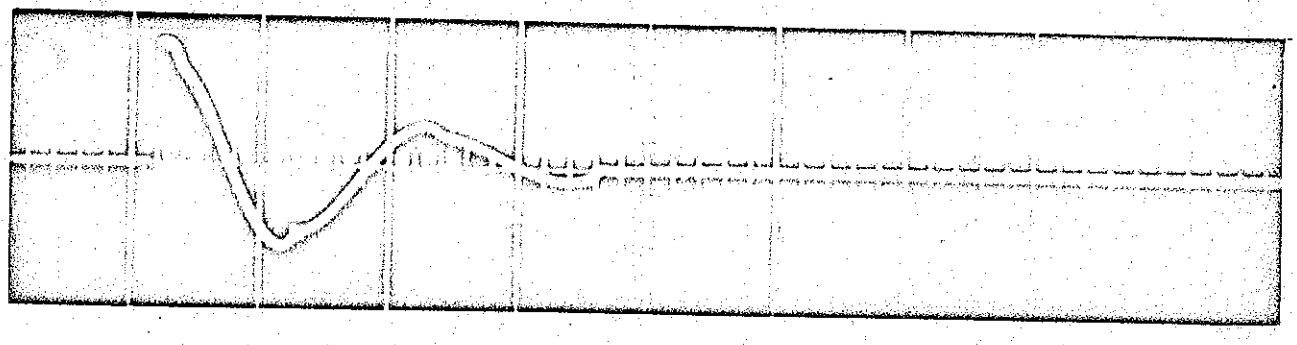

Figure 30. Calibration test load voltage -- large diameter phenolic flyer plate experiment (250 volts per division; 10 microseconds per division).

EG&G INC.

corresponds to an angular-ringing frequency of 3×10^5 sec^{-1} (47.8 kilohertz).

The inductance of the workpiece cannot be determined in the straight-forward manner previously used. As the flyer plate does not extend over the entire 10-inch length of the flux concentrator, the area of the insulation gap is not the same for any cross section. The inductance can be simply obtained by dividing the workpiece into five equal two-inch lengths, the middle section containing the flyer plate, and then computing the inductance of each section. The inductance of the entire workpiece is then the sum of these five inductances in parallel.

The minimum inductance that can be achieved with a given workpiece is limited by the skin depth of the time-varying currents and fields in the metal that comprises the workpiece. Since the flux concentrator and the flyer plate are made of aluminum, the minimum effective physical separation between the two is twice the skin depth in aluminum at the circuit frequency. Decreasing the separation beyond this distance will not measurably change the inductance.

The skin depth in aluminum at 47.8 kilohertz is 15.5 mils, which is greater than the distance between adjacent metal surfaces of the workpiece. Thus, in calculating the inductance of a given section of the workpiece, bear in mind that when computing the insulation gap area, the minimum effective physical separation is 31 mils.

The cross-sectional view of the two-inch section of workpiece containing the flyer plate is shown in Figure 31.

The inductance of this section is

$$L_o = \frac{4\pi}{\ell} \left(2\pi a_1 \Delta + \frac{4}{3} \pi a_2 \Delta + \frac{2}{3} \pi R_f \Delta + s^2\right) \qquad (27)$$

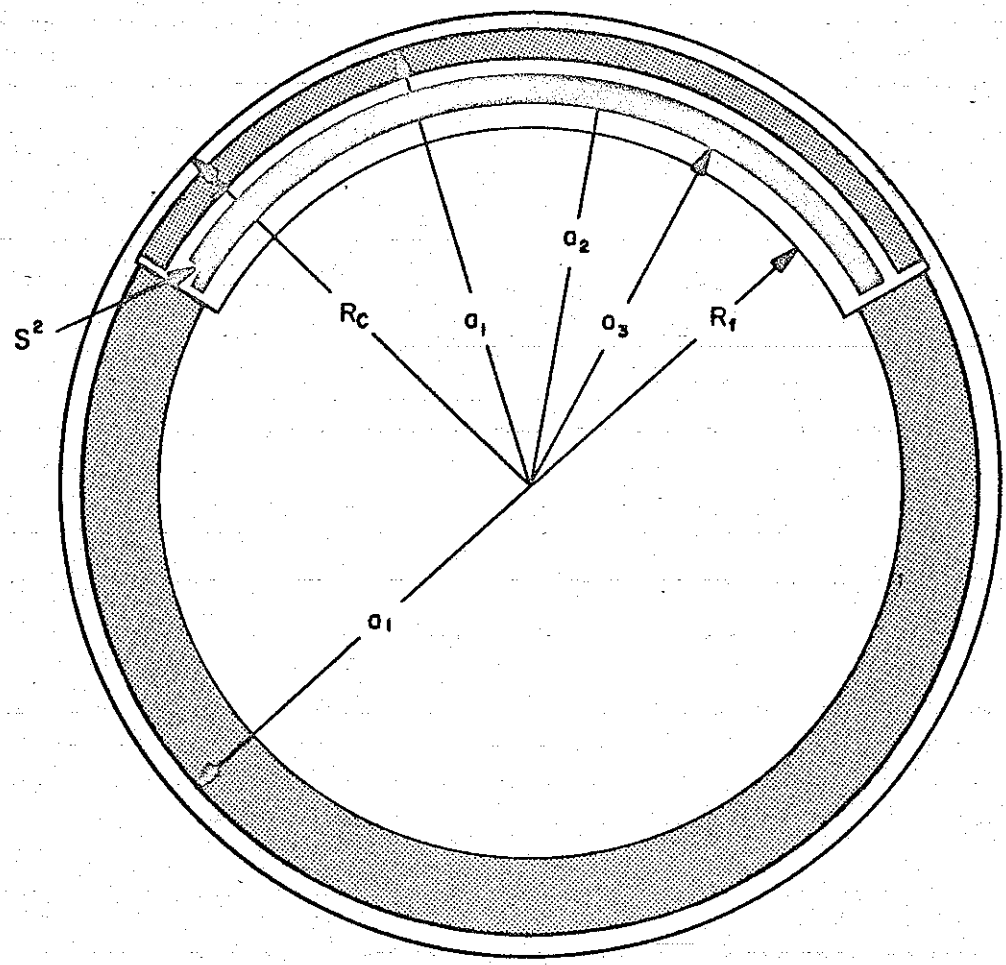

Figure 31. Cross-sectional view of center section of workpiece -- large diameter phenolic flyer plate experiment.

where a_1 is the outer radius of both the 240-degree section and of the outermost insert between the flux concentrator and flyer plate, a_2 is the outer radius of the insert adjacent to the flyer plate, s^2 is the cross-sectional area of the square hole, and Δ is the minimum separation of twice the skin depth.

The term a_2 in Equation (27) contains an additional factor of two to include the leakage inductance between the two inserts.

One finds for $a_1 = 12.880$ centimeters, $a_2 = 10.950$ centimeters, $R_f = 9.032$ centimeters, $s^2 = 0.953$ square centimeter, and $\Delta = 7.88 \times 10^{-2}$ centimeter,

$$L_o = 30.5 \text{ nH}$$

Each of the other four sections has a much larger inductance because of the absence of the flyer plate and the correspondingly increased area of the air gap. Denoting the inductance of any one of these sections by L_1,

$$L_1 = \frac{4\pi}{\ell}\left(2\pi a_1 \Delta + \frac{4}{3}\pi a_2 \Delta + \frac{\pi}{3} a_3^2\right) \tag{28}$$

where $a_3 = 9.045$ centimeters is the inner radius of the innermost insert. One finds the $L_1 = 235.2$ nanohenries.

The parallel combination of these 5 inductances (L_o and 4 equal inductances L_1) thus constitutes the inductance of the workpiece.

$$L_w = \frac{\frac{1}{4} L_1 L_o}{\frac{1}{4} L_1 + L_o} \tag{29}$$

and for the values of L_o and L_1 computed above, $L_w = 20.0$ nanohenries.

The workpiece inductance can also be obtained from the ringing frequency and the damping rate. The latter quantity can be calculated from either of the two voltage traces by taking the ratio of voltages of successive peaks. This process leads to a value of $a = 6 \times 10^4 \text{ sec}^{-1}$.

The total circuit inductance, L, is then related to these two parameters by

$$L = \frac{1}{C(\omega^2 + a^2)} = 65 \text{ nanohenries}$$

and finally, subtracting the bank inductance, L_B, from this value,

$$L_w = L - L_B = 20 \text{ nanohenries},$$

which agrees with the result computed above.

With L_w known, the inductance of the pickup loop is again computed from the following:

$$\frac{L_p}{L_w} = \frac{V_p}{V_L} .$$

Examination of the two voltage traces revealed an average voltage ratio of 36.7. Thus, $L_p = \frac{L_w}{36.7} = 0.55$ nanohenry is the proper calibration factor.

4.3.2 Determination of the Current and Magnetic Pressure Impulse. During the actual experiment, the bank was discharged at a voltage of 19.4 kilovolts. Photographs taken with the Kerr Cell camera during another, nearly identical, test without the test sample present revealed an average maximum velocity of 5×10^4 cm/sec for the flyer plate.

The appropriate voltage traces are displayed in Figures 32 and 33. The initial value of V_L provides still another method of determining the workpiece inductance. At t = 0, the entire bank voltage is distributed between the two inductances in the circuit. The ratio of L_w to the total circuit inductance, L, must equal the ratio of V_L at t = 0 to the bank voltage, V_o, since

$$V_o = (L_B + L_w) \left(\frac{dI}{dt} \right)_{t = 0}$$

and

$$V_L (t = 0) = L_w \left(\frac{dI}{dt} \right)_{t = 0} . \qquad (30)$$

The load voltage has an initial value of 5.80 kilovolts, and one again obtains the same value: L_w = 20 nanohenries.

Values of V_L, V_p, and dI/dt are listed below in Table 5. The inductance of the workpiece, with the elimination of the multiple-turn coil, now represents a greater proportion of the total circuit inductance than in the previous cases, thus accounting for the increased magnitude of the load voltage.

Note the considerable phase difference between the two voltages. After one period, dI/dt leads V_L by a full 4 microseconds, which implies the presence of a rather large resistive voltage component. This is not surprising as the several return current paths present in the workpiece account for a relatively high resistance of 2.8 milliohms. (In either of the two previous examples, R_L was not greater than 0.5 milliohm.)

The current is again obtained from dI/dt by numerical integration and is plotted in Figure 34. The maximum current of 700 kiloamps occurs at approximately 4.5 microseconds.

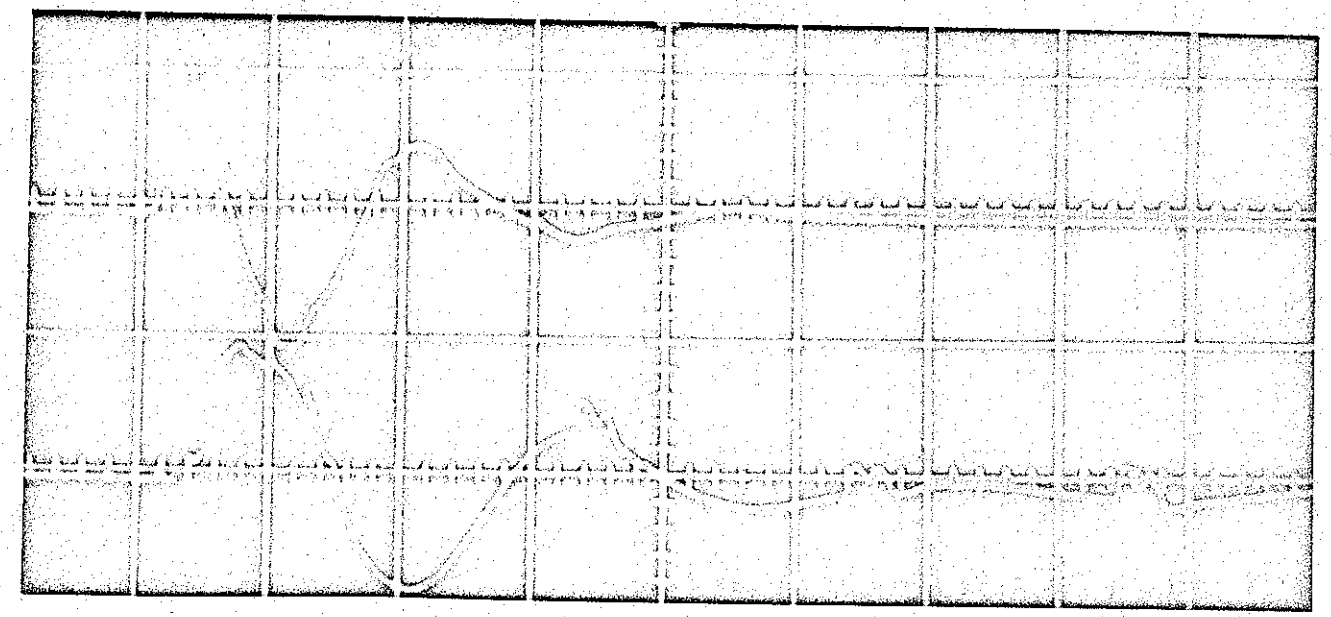

Figure 32. Loop voltage -- large diameter phenolic flyer plate experiment (100 volts per division; 10 microseconds per division).

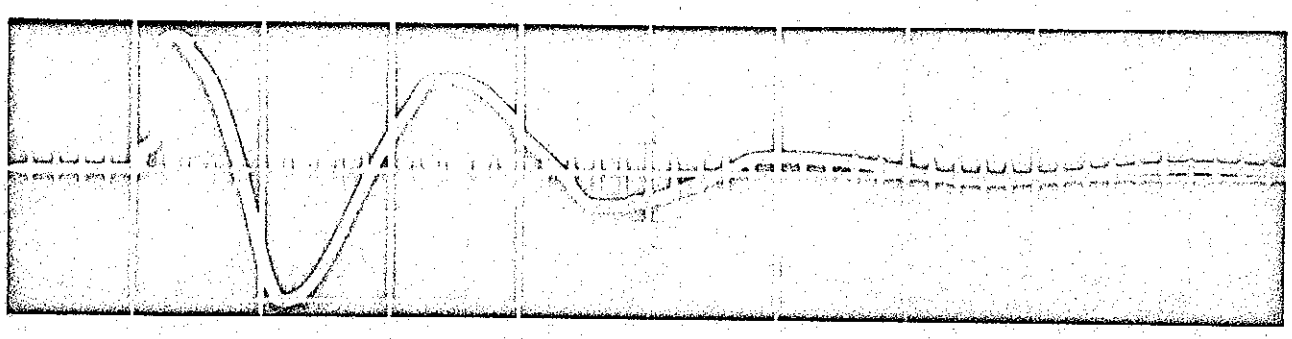

Figure 33. Load voltage -- large diameter phenolic flyer plate experiment (5 kilovolts per division; 10 microseconds per division).

EG&G INC.

TABLE 5. VALUES RECORDED FROM VOLTAGE TRACES -- LARGE DIAMETER PHENOLIC FLYER PLATE EXPERIMENT

time (μsec)	V_L (kV)	V_p (volts)	$\frac{dI}{dt}$ $\left(\frac{kA}{\mu sec}\right)$
0	5.80	143	2.55
1.0	5.15	127	2.27
2.0	4.85	98	1.75
3.0	4.15	66	1.18
4.0	3.45	26	0.46
5.0	2.40	-9	-0.15
6.0	0.80	-39	-0.70
7.0	-0.85	-62	-1.11
8.0	-2.75	-90	-1.61
9.0	-4.35	-103	-1.83
10.0	-5.00	-100	-1.79
11.0	-4.80	-74	-1.32
12.0	-4.35	-62	-1.11
13.0	-3.65	-43	-0.77
14.0	-2.70	-23	-0.41
15.0	-1.65	-1	-0.02
16.0	-0.70	27	0.48
17.0	0.35	40	0.71
18.0	1.25	50	0.89
19.0	2.00	53	0.95
20.0	2.75	50	0.89
21.0	3.40	40	0.71
22.0	3.55	28	0.50
23.0	3.55	20	0.36
24.0	3.45	13	0.23
25.0	3.25	8	0.14
26.0	2.85	2	0.04
27.0	2.35	-3	-0.05
28.0	1.80	-8	-0.14

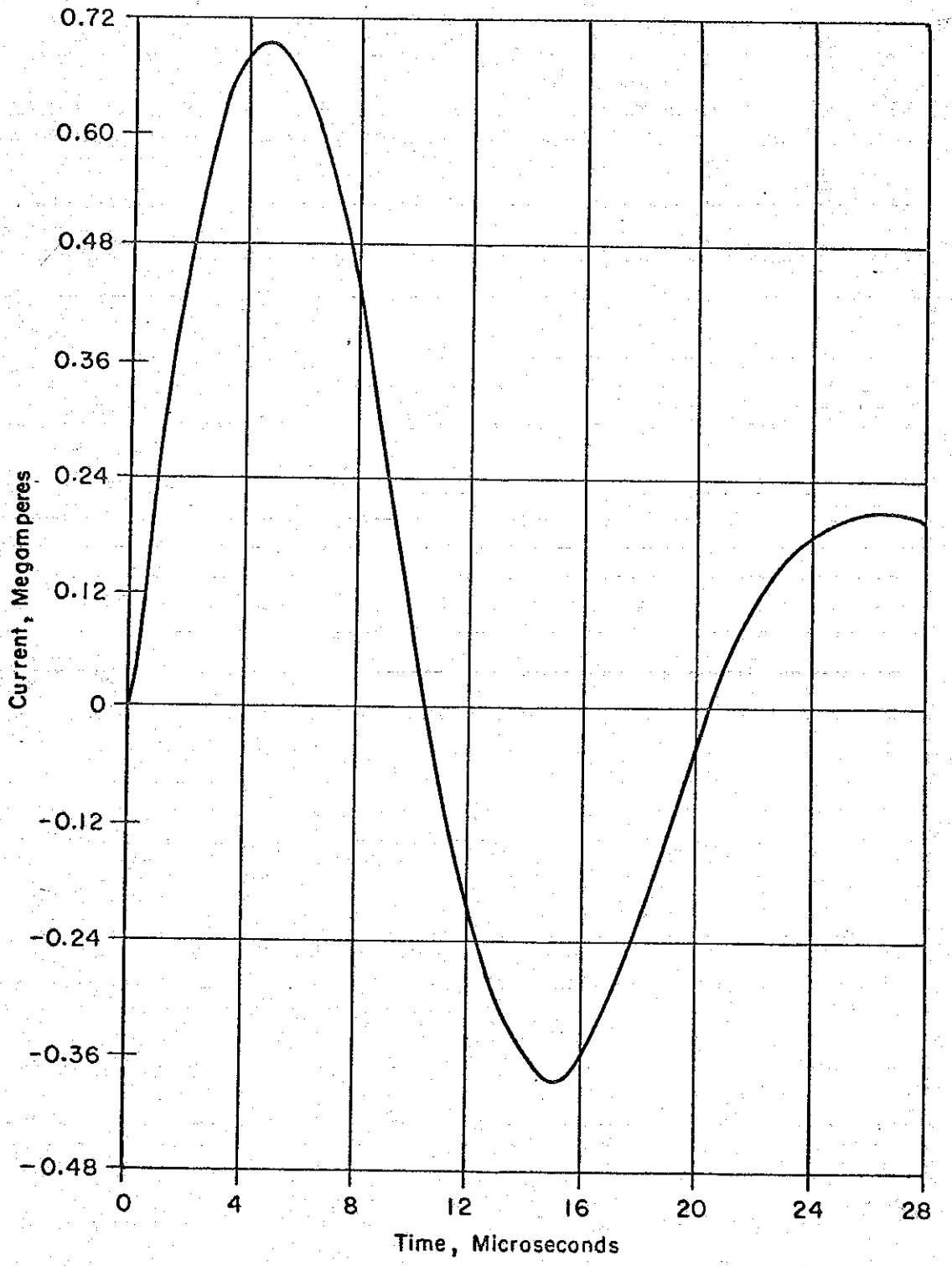

Figure 34. Current through workpiece -- large diameter phenolic flyer plate experiment.

The shorter 2-inch length of the flyer plate results in a peak magnetic pressure in excess of one kilobar (1.18 kilobars), which is illustrated in Figure 35. Previous peak pressures did not exceed 0.7 kilobar.

The values of the magnetic pressure impulse are also correspondingly higher. The impulse is plotted as a function of time in Figure 36. Note that more than 90 percent of the total loading has occurred during the first 18 microseconds.

Again, one can obtain the flyer-plate velocity by equating the impulse to the momentum per unit area of the flyer plate. The mass per unit area of the flyer plate is

$$m = \rho_A h_A + \rho_p h_p \qquad (31)$$

where the subscripts A and p denote aluminum and phenolic, respectively.

The flyer plate consisted of a 24-mil thickness of phenolic backed with an 11-mil thickness of aluminum. The thickness of aluminum was chosen so as to provide maximum acceleration of the flyer plate for a given magnetic pressure. From Newton's Second Law, the acceleration of the flyer plate produced by the magnetic pressure is

$$a = P/M \qquad (32)$$

where m is again the mass per unit area of the flyer plate.

The magnetic field lines, which are initially located at the outer boundary of the aluminum part of the flyer, penetrate the metal over a distance determined by the skin depth, δ. If h_A is the thickness of aluminum, the fraction of the total field, B, which penetrates completely

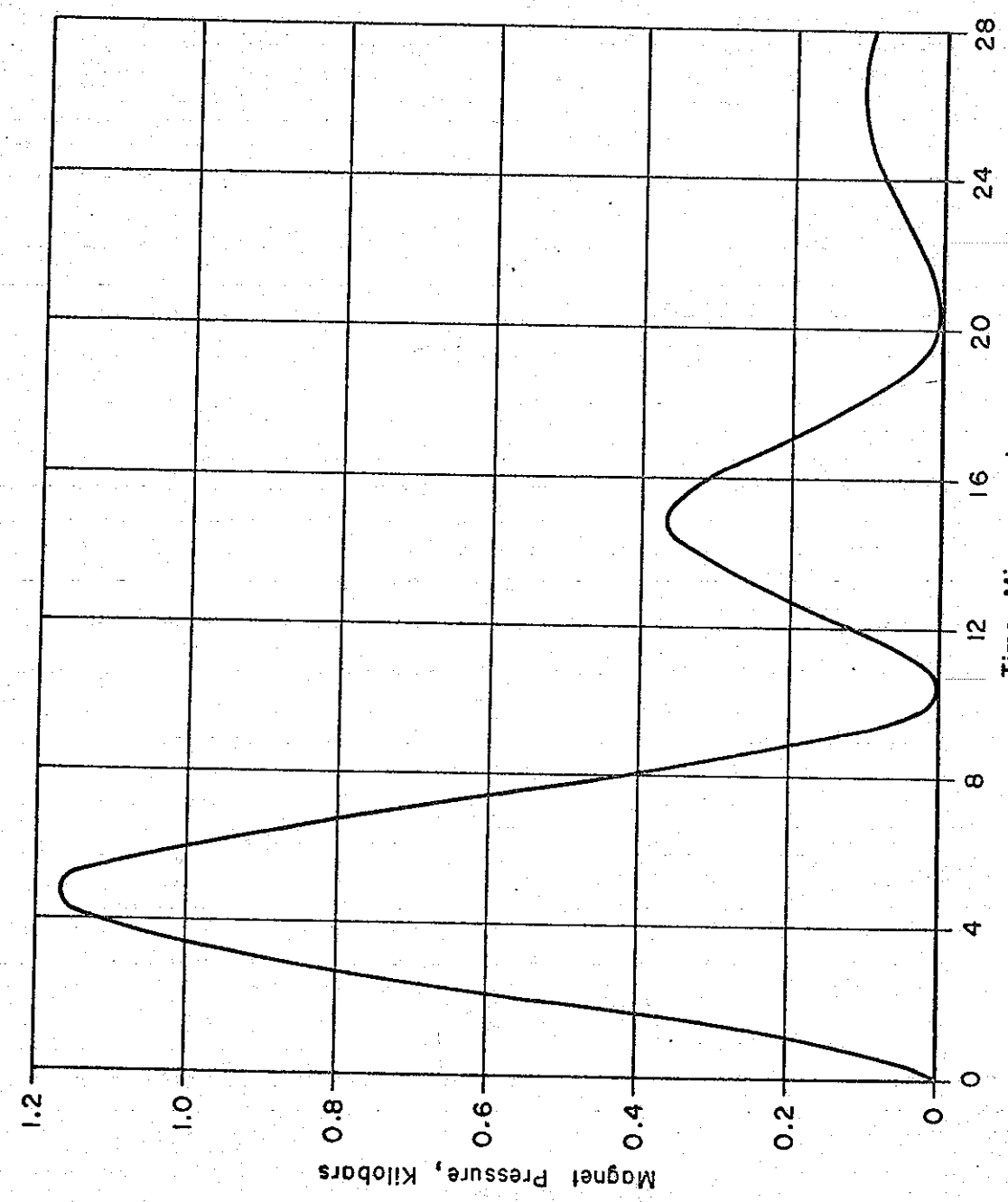

Figure 35. Magnetic pressure incident on flyer plate -- large diameter flyer plate experiment.

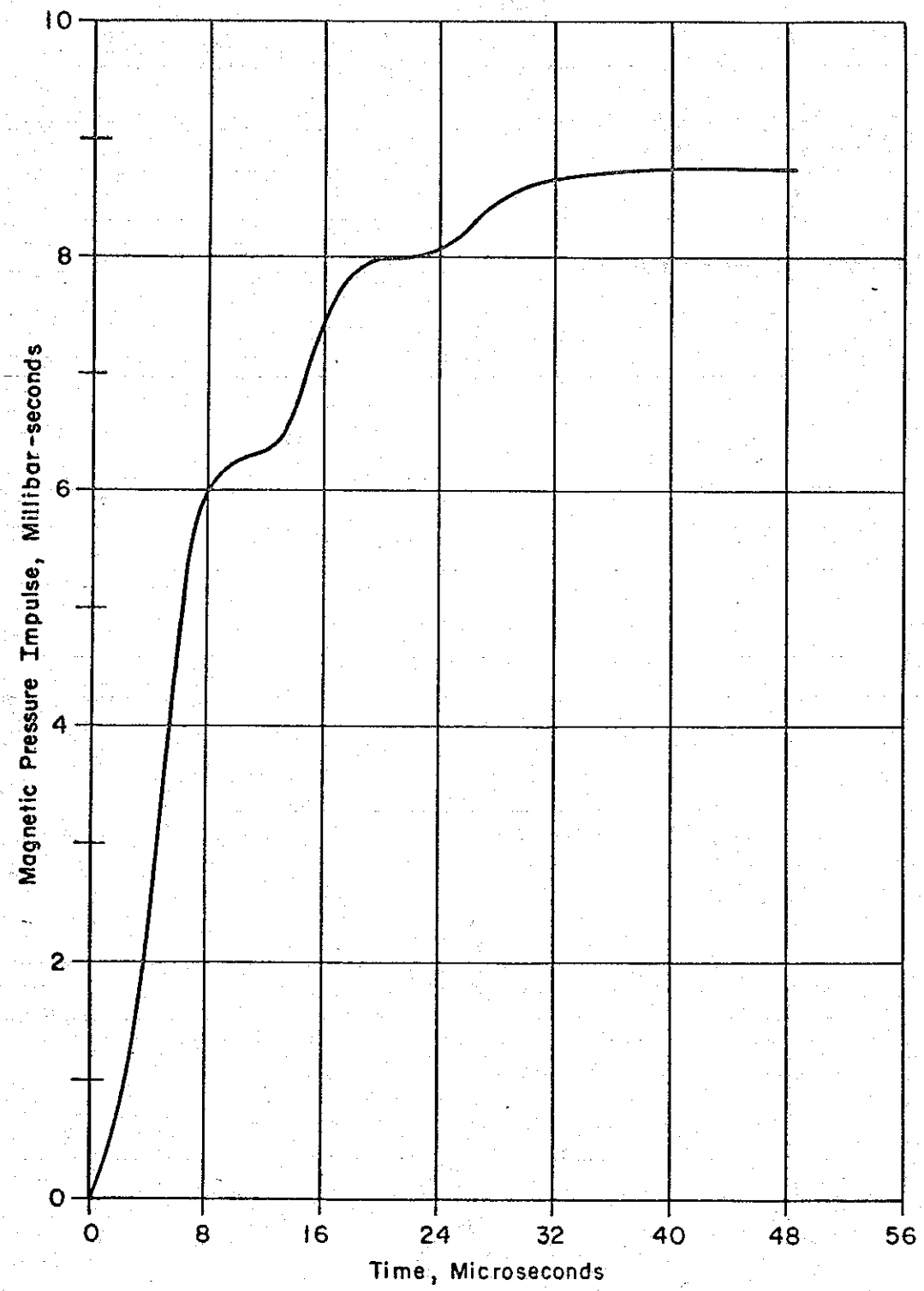

Figure 36. Magnetic pressure impulse -- large diameter phenolic flyer plate experiment.

through the aluminum, is given approximately by $e^{-h_A/\delta}$. As the magnetic pressure is proportional to B^2, the magnetic field still contained within the aluminum gives rise to a pressure

$$P = P_o\left(1 - e^{-2\frac{h_A}{\delta}}\right). \tag{33}$$

Equation (31) gives the mass per unit area. For $h_p = 6.1 \times 10^{-2}$ cm (24 mils),

$$m = 2.7\, h_A + 8.23 \times 10^{-2} \text{ gm/cm}^2 \tag{34}$$

and then, substituting the results of Equations (33) and (34) in (32),

$$a = \frac{P_o\left(1 - e^{-2\frac{h_A}{\delta}}\right)}{2.7\, h + 8.23 \times 10^{-2}}. \tag{35}$$

Differentiating this last result with respect to h_A and setting the derivative to zero, one can then solve for the thickness h_A which maximizes the acceleration. The result of interest is

$$e^x = x + 2.5 \tag{36}$$

where

$$x = 2\frac{h_A}{\delta}.$$

The solution of this transcendental equation yields $x = 1.35$, and hence, $h_A = \frac{x\delta}{2} = 10.5$ mils, thereby dictating the choice of an 11-mil thickness of aluminum.

The impulse has a magnitude of 8.7×10^3 dyne-sec/cm^2 after 30 microseconds. For a mass of 0.157 gm/cm^2,

$$v_f = \frac{\Gamma}{m} = 5.6 \times 10^4 \text{ cm/sec}$$

only a factor of two less than the desired value of 10^5 cm/sec.

However, since the initial separation between the flyer plate and the test sample was only 55 mils (0.128 centimeter) the flyer plate traversed this distance in a time shorter than 30 microseconds and consequently struck the test sample before it had been accelerated to the maximum obtainable velocity. Assuming that the velocity as a function of time can be approximately obtained from the time history of the impulse, one obtains the values listed in Table 6 below.

TABLE 6. FLYER-PLATE VELOCITY

time (μsec)	v_f $\left(\frac{\text{mm}}{\mu\text{sec}}\right)$
1	0.016
2	0.044
3	0.088
4	0.135
5	0.210
6	0.303
7	0.352
8	0.373
9	0.386
10	0.391
11	0.394
12	0.395

The distance, moved by the flyer plate accelerated from rest, is

$$d = \int_{o}^{t} v_f(t')dt' \quad . \tag{37}$$

This distance is obtained from the velocity by numerical integration. One finds that after 8 microseconds, the flyer plate has moved a total distance of 0.13 centimeter, which was the initial separation between the flyer plate and the test cylinder. Thus, from the values in Table 6, one can conclude that the flyer plate achieved a velocity of 3.7×10^4 cm/sec just prior to impact.

4.3.3 Determination of the Time-Varying Inductance. Unlike the preceding experiments, this workpiece was designed so that only the flyer plate was set into motion by the action of the magnetic pressure. Therefore, as was previously mentioned, it is then theoretically possible to relate the time rate of change of the workpiece inductance directly to the flyer-plate velocity. In practice, other complications are present here that greatly reduce the effectiveness of this method. As the flyer plate and the inner aluminum insert are initially separated by 5 mils, which is considerably less than two skin depths, the motion of the flyer plate will not be reflected in a significant change in L_w until this separation has increased to 31 mils. Furthermore, additional motion of the flyer plate produces very small changes in L_w. When the flyer plate has struck the test cylinder, it has moved a distance of 55 mils from its initial position. This increases the inductance of the middle section of the workpiece, L_o, by only 3.7 nanohenries from its initial value of 30.5 nanohenries and, in turn, changes the entire workpiece inductance by only 1.7 nanohenries from its initial value of 20 nanohenries. In order to determine the velocity-time profile from such small changes in L_w, it would be necessary to

compute L_w to much greater accuracy than can presently be achieved.

The time-varying inductance was determined in the usual manner:

$$L_w = \int_0^t \frac{(V_L - IR_L)\, dt'}{I}$$

with R_L = 2.8 milliohms.

Values of L_w are listed in Table 7 below. Note that there is no appreciable change in inductance over the first three microseconds. One can reliably predict that during this time interval, the separation between flyer plate and insert was still much less than 31 mils. The values in Table 6 seem to indicate that the flyer plate struck the cylinder after approximately 8 or 9 microseconds, which substantiates the result of Section 4.3.2.

TABLE 7. VARIATION OF WORKPIECE INDUCTANCE WITH TIME

time (μsec)	L_w (nH)
0	19.9
1	19.9
2	20.0
3	20.2
4	20.8
5	21.2
6	21.4
7	21.6
8	21.8
9	21.8

4.3.4 Efficiency of the System. The maximum theoretical efficiency, which represents the fraction of the total bank energy that is stored in the magnetic field of the workpiece and is thus available to perform work on the flyer plate, is

$$\eta_{max} = \frac{L_w}{L} \exp\left(-2 \frac{a}{\omega} \tan^{-1} \frac{\omega}{a}\right) . \quad (38)$$

For $\omega = 3 \times 10^5$ sec^{-1} and $a = 6 \times 10^4$ sec^{-1}, η_{max} equals 19.3 percent.

It is not possible to determine the actual work done on the flyer plate by evaluating the integral

$$W_s = \frac{1}{2} \int \frac{dL_w}{dt'} I^2 dt' \quad (39)$$

because, as was discussed above, the motion of the flyer plate is not always associated with a change in inductance of the workpiece.

The actual kinetic energy of the moving flyer plate can be estimated, however. The flyer plate has a mass per unit area of 0.157 gram per square centimeter, a surface area of 95.8 square centimeters, and hence a total mass of 15 grams. The kinetic energy, at a velocity of 3.7×10^4 cm/sec (as determined previously), is

$$K = \frac{1}{2} M v_f^2 = 1.1 \text{ kilojoules.}$$

As the total bank energy, E_o, is 31.4 kilojoules, this kinetic energy represents an actual efficiency of $\eta = \frac{K}{E_o} = 3.5$ percent.

The major portion of the energy stored in the magnetic field of the coil assembly is dissipated in Joule heating, since the actual efficiency

is less than one-fifth of the maximum attainable value. The workpiece can be re-designed so as to reduce the number of return current paths and simultaneously decrease the workpiece resistance. This will be discussed in Chapter 5.

From the previous work reported here and in Reference 2, it has been determined that the existing EG&G 33-kilojoule Pulse Power Bank can be used to meet some of the technical objectives of this project.[1] It can provide impulsive magnetic field loading over flat surfaces and selected sectors of cylindrical surfaces with certain restrictions. The objective of achieving flyer-plate velocities on the order of 10^5 centimeters per second can be achieved only if the length of the flyer plate is restricted to about 2 inches. The required impulse can be achieved only with careful attention to minimizing the inductance and resistance added to the system by the workpiece. Good simultaneity of impact can be realized in cylindrical geometry only if the distance of travel before impact is limited to 2 or 3 percent of the initial radius.

To satisfy these restrictions, a new load coil has been fabricated; see Figure 37. The inside radius of the cylindrical sector is 3.1 inches. The lengths of all pieces are 6 inches. The assembly has been designed to accommodate cylindrical test samples of approximately 6-inch outside diameter. Aluminum flyer plates of selected lengths will be clamped, as shown in Figure 37. Test samples of the same length will be mounted off the flyer plate at a suitable distance by small spacers at each end of the 120-degree sector. The spacer thickness chosen will depend upon the results of velocity data obtained from high-speed photography of the flyer-plate motion in the absence of a test sample.

Initial impulsive loading tests will involve the impact of 0.010-inch aluminum flyer plates on 6-inch OD aluminum cylinders, both having a 2-inch length. For the initial tests, aluminum tubing with wall thicknesses of 0.049, 0.083, 0.125 and 0.250 inches have been procured.

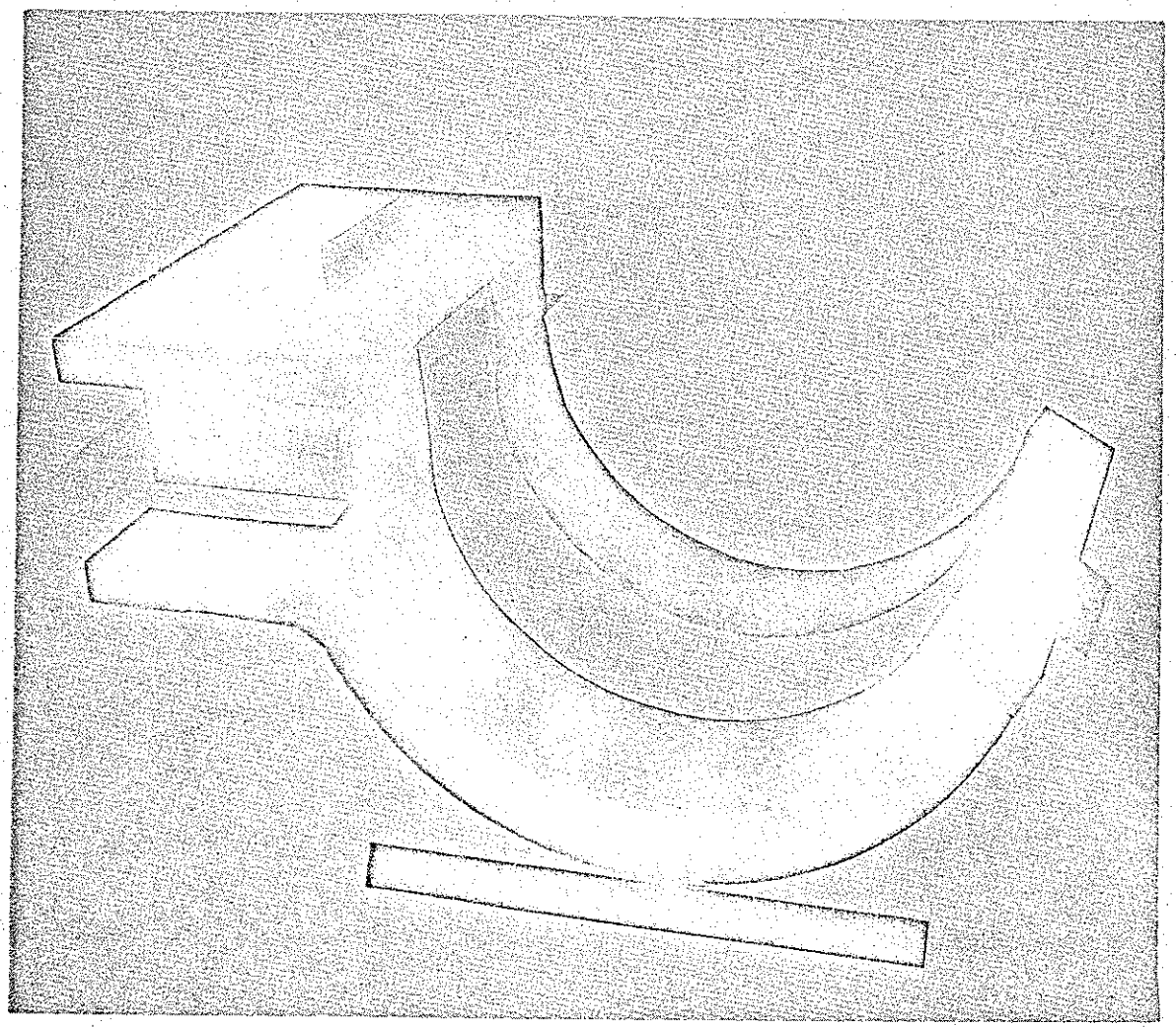

Figure 37. Low-inductance 120-degree load coil.

EG&G INC.

1. Private communication from Sandia Corporation to Dr. R. C. O'Rourke of Edgerton, Germeshausen & Grier, Inc,; "Shock and Impulsive Loading of Materials and Structures"; 7 October 1965.

2. O'Rourke, R. C., C. B. Dobbie, S. Protopapa, L. E. Smollen, C. O. Phillips, Jr. and J. Z. Farber; "Progress Report, Impulsive Load Tests on Cylindrical Assemblies, Phase 1"; B-3147; Edgerton, Germeshausen & Grier, Inc., Boston, Massachusetts; 24 September 1965; p. 48.

3. Ibid., p. 15

4. Ibid., pp. 21-23.

5. Ibid., pp. 3-11.